

**EFFECTS of FREQUENCY-TIME OFFSETS on SMART ANTENNA  
ALGORITHMS for W-CDMA**

by  
**ERCÜMENT ZORLU**

Submitted to the Graduate School of Engineering and Natural Sciences  
in partial fulfillment of  
the requirements for the degree of  
Master of Science

Sabanc University  
Spring 2003

EFFECTS of FREQUENCY-TIME OFFSETS on SMART ANTENNA  
ALGORITHMS for W-CDMA

APPROVED BY

Assist. Prof. Dr. İbrahim TEKİN .....  
(Thesis Supervisor)

Assist. Prof. Dr. Mehmet KESKİNÖZ .....

Assist. Prof. Dr Yaşar GÜRBÜZ .....

DATE OF APPROVAL: .....

EFFECTS of FREQUENCY-TIME OFFSETS on SMART ANTENNA  
ALGORITHMS for W-CDMA

**Abstract**

The CDMA and smart antennas are two promising approaches to increase system capacity and spectrum efficiency for mobile communication services. In a CDMA system, frequency offset between local oscillator and the carrier of impinging signal, timing offset between local generated PN sequence and received PN sequence, imperfect power control may exist and this degrades the performance of the smart-antenna algorithms. In this thesis, the effects of frequency and timing offsets on smart antenna performance is presented. A smart antenna system has been set up to implement blind adaptive algorithms for W-CDMA in a laboratory environment. The blind adaptive algorithms implemented on the smart antenna system are Least- Squares Despread-Respread Multi Target Array (LS-DRMTA) and Least- Squares Despread-Respread Multi Target Constant Modulus Algorithm (LS-DRMTCMA). Since both LS-DRMTA and LS-DRMTCMA algorithms utilize users PN sequence, they have several advantages compared to other blind adaptive algorithms for CDMA. BER and beamforming performances of LS-DRMTA and LS-DRMTCMA algorithms in a two-user and two- element-antenna array system is evaluated for systems with timing offset and frequency offset. Experimental results show that frequency and timing offset degrades the performance, however they still give reasonable BER. In all test conditions LS-DRMTA and LS-DRMTCMA outperforms conventional receiver, moreover LS - DRMTCMA can generate deeper nulls and outperforms LS-DRMTA.

## Table of Contents

Abstract	iii
<b>1 Introduction</b>	<b>1</b>
<b>2 Introduction to Adaptive Antenna Arrays and Beamforming</b>	<b>4</b>
2.0.1 Switched-beam Systems	9
2.0.2 Adaptive Arrays	10
2.1 Smart Antenna Algorithms	13
2.1.1 Direction of Arrival-Based Beamforming	13
2.1.2 Temporal Reference-Based Beamforming (TRB)	19
2.1.3 Signal-Structure Based Beamforming (SSBF)	21
2.2 Implementation Aspects of Smart Antenna Systems	24
<b>3 Smart Antenna Algorithms Used in CDMA system</b>	<b>25</b>
3.1 Introduction	25
3.2 W-CDMA	26
3.3 Smart Antenna Algorithms for CDMA Systems	28
3.3.1 Least Squares De-spread Re-spread Multitarget Array	30
3.3.2 Least Squares De-spread Re-spread Multitarget Constant Modulus Algorithm	31
<b>4 Results and Discussions</b>	<b>35</b>
4.1 Introduction	35
4.2 The Smart Antenna Test-Bed	35
4.3 Results	38
4.3.1 BER Performance without Frequency and Timing Offset	39
4.3.2 BER Performance with Timing Offset	42
4.3.3 BER Performance with Frequency Offset	44

5	Conclusion	52
	Bibliography	55

## List of Figures

2.1	Some of the array configurations. (a)Circular (b) Linear (c) Planar . . . . .	4
2.2	Typical linear array structure. . . . .	5
2.3	A plane wave incident on a ULA from direction $\theta$ . . . . .	7
2.4	A wide band beamformer. . . . .	9
2.5	Beampatterns for an equal-weight, 8 element ULA beamformer for different $\frac{d}{\lambda}$ . . . . .	10
2.6	A Butler matrix. . . . .	11
2.7	Adaptive array. . . . .	12
3.1	W-CDMA spreading and power spectrum. . . . .	27
3.2	Code tree for generation of OVSF codes. . . . .	29
3.3	Uplink spreading and de-spreading for W-CDMA having carrier fre- quency $w_0$ . . . . .	30
3.4	Structure of a BF using LS-DRTMA. . . . .	32
3.5	LS-DRMTA block diagram. . . . .	33
3.6	Structure of a BF using LS-DRMTCMA. . . . .	34
3.7	LS-DRMTCMA block diagram. . . . .	34
4.1	The test-bed includes two transmitters and a receiver system. . . . .	36
4.2	The transmitter. . . . .	37
4.3	The receiver system. . . . .	38
4.4	(a) Baseband I channel output of the first antenna. (b) Baseband I channel output of the second antenna. (c) Combined signal. In this case SIR = - 8dB, the angle between SOI and interferer is $45^0$ . . . . .	39

4.5	Antenna array pattern corresponding to the weights computed by LS-DRMTA and LS-DRMTCMA. In this figure the angle separation is $45^0$ , and SIR = -4dB. . . . .	40
4.6	BER vs. SIR of conventional receiver and LS-DRMTA for different angle separations. . . . .	41
4.7	BER performance of conventional receiver and LS-DRMTCMA for different angle separations . . . . .	42
4.8	BER performance of LS-DRMTA and conventional receiver in %25 timing offset case. . . . .	44
4.9	BER performance of LS-DRMTCMA and conventional receiver in %25 timing offset case. . . . .	45
4.10	BER vs. timing offset . In this figure SIR = -8dB and angle separation is $45^0$ . . . . .	47
4.11	Array patterns for different timing offsets. (a) $T_o = 0$ , (b) $T_o = \%25T_c$ , (c) $T_o = \%50T_c$ , (d) $T_o = \%75T_c$ , (e) $T_o = \%100T_c$ . In this figure SIR = -10 dB and angle separation is $45^0$ . . . . .	48
4.12	(a) QPSK Constellation. (b) Rotated QPSK constellation due to frequency offset. . . . .	48
4.13	BER performance of conventional receiver and LS-DRMTA. In this figure the frequency offset is 100 Hz and $\phi_a$ is set at $0.1\pi$ . . . . .	49
4.14	BER performance of conventional receiver and LS-DRMTCMA. In this figure the frequency offset is 100 Hz and $\phi_a$ is set at $0.1\pi$ . . . . .	49
4.15	BER vs frequency offset. In this figure, angle separation between the users is $45^0$ , SIR = -4 dB and $\phi_a$ is set at $0.1\pi$ . . . . .	50
4.16	BER vs $\phi_a$ for the LS-DRMTA algorithm. In this figure, SIR = -4 dB, the angle separation is $30^0$ and $45^0$ . . . . .	51
4.17	BER vs $\phi_a$ for the LS-DRMTCMA algorithm. In this figure, SIR = -4 dB, the angle separation is $30^0$ and $45^0$ . . . . .	51

## List of Tables

4.1	BER values in the case without timing and frequency offset. . . . .	43
4.2	BER values in %25 timing offset case . . . . .	46
4.3	BER values in frequency offset case. In this table frequency offset is 100 Hz. . . . .	50

# Chapter 1

## Introduction

In the future there will be a huge demand for mobile communication services that requires high capacity communication systems. The 3<sup>rd</sup> generation (3G) systems are based on wideband CDMA (W-CDMA) technology to satisfy the increasing demand for mobile communication services [1]. To increase the system capacity further, some techniques that reduces the co-channel interference (CCI) in the W-CDMA system must be implemented, since interference is the major contributor that reduces the capacity of a W-CDMA system. Smart antennas is such an approach that eliminates the CCI by locating the nulls in the direction of the interferers while steering the main lobes toward the desired mobile [2]. Smart antenna system is an adaptive antenna array that comprises an antenna array and beamforming module that calculates the antenna weights using smart antenna algorithms.

Frequency offset, timing offset between local generated PN sequence and received PN sequence and imperfect power control are the three major factors that can degrade the performance of the smart antenna algorithms for CDMA systems. The aim of this thesis is to investigate the effects of timing and frequency offset. For that reason a smart antenna system has been set up to implement blind adaptive algorithms for W-CDMA in a laboratory environment. The set up is a simple implementation of a W-CDMA system that consists of two transmitters, representing two mobile users, and a receiver system. One of the transmitters represents the desired user and the other one is the interferer. In the receiver system, a half-wavelength spaced two-element antenna array is used, and each array element is connected to

a different digital receiver that makes the conversion from RF to baseband . The output of the receivers, sampled and digitized baseband data, is sent to a computer to implement the smart antenna algorithms.

Since, multiple users share the same RF band in a CDMA system, the algorithms should be multitarget-type algorithms having the ability to separate and extract each user's signal simultaneously. There are four main blind smart antenna algorithms,

- Multitarget Least Squares Constant Modulus Algorithm (MT-LSCMA) [3]
- Multitarget Decision-Directed (MT-DD) Algorithm [4]
- Least- Squares De-spread Resepread Multitarget Array (LS-DRMTA) [4]
- Least- Squares De-spread Resepread Multitarget Constant Modulus Algorithm (LS - DRMTCMA). [4]

These algorithms are blind since there is no need to use training signal. LS-DRMTA and LS - DRMTCMA developed by Rappaport and Rong [4], and implemented in our test-bed.

This thesis is organized as follows. Chapter 2 introduces the basic concepts of adaptive antenna arrays and beamforming, then overviews smart antenna algorithms. Beamforming is discussed in two parts as switched-beam systems and adaptive arrays. Smart antenna algorithms are explained in three subsections as direction of arrival-based beamforming, temporal-reference beamforming and signal-structure based beamforming. In direction of arrival-based beamforming section, direction of arrival-based algorithms and direction of arrival (DOA) estimation techniques are introduced. In temporal-reference beamforming section, Least Mean Square (LMS) and Recursive Least Squares (RLS) algorithms are examined. In signal-structure based beamforming section, constant modulus algorithm (CMA) and Least-Squares CMA (LS-CMA) algorithms are presented. Finally implementation aspects of smart antennas are discussed briefly.

In Chapter 3, key specifications of W-CDMA and W-CDMA uplink is discussed briefly since in our test-bed only the W-CDMA uplink is used. In the following sections, smart antenna algorithms for CDMA systems, MT-LSCMA, MT-DD, LS-DRMTA and LS-DRMTCMA, are presented . MT- LSCMA utilizes the constant modulus property of the transmitted signal in a CDMA system, and uses LS-CMA. MT-DD employs decision directed (DD) algorithm, i.e detected symbols are used as reference signal for beamforming. LS-DRMTA utilizes spreading signal of each user used in CDMA system. LS-DRMTCMA utilizes both spreading signal of each user and constant modulus property of the transmitted signal in a CDMA system. The properties, advantages and disadvantages of these algorithms are discussed in this chapter.

In chapter 4, the properties of the set-up is presented in the first section. The properties of the receivers, transmitters, and the structure of the transmitted signal are given in this section. Then, the outputs of the set-up are analysed. Bit error rate (BER) performance of LS-DRMTA, LS-DRMTCMA and conventional receiver are compared in three cases. BER performance without frequency and timing offset case, BER performance in timing offset case, BER performance in frequency offset case are discussed in this chapter.

A brief summary and conclusions are provided in Chapter 5.

## Chapter 2

### Introduction to Adaptive Antenna Arrays and Beamforming

Antenna arrays is the crucial part of the beamformers, since it generates the directional antenna pattern. In an antenna array several antennas are arranged in space to produce a directional radiation pattern. Each element of the array may be fed with excitation currents having different phase and amplitude. The elements then combine with different phases in the far field, and then the radiation pattern can be controlled.

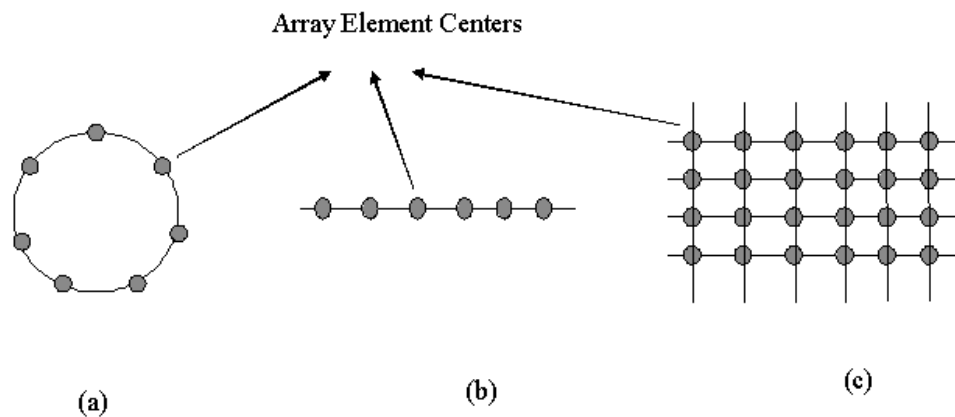


Figure 2.1: Some of the array configurations. (a)Circular (b) Linear (c) Planar

Arrays can be arranged in various geometrical configurations as shown in Figure 2.1. The most basic and elementary array structure is Uniform Linear Array (ULA),

, depicted in Figure 2.1.a.

control.

In the array if identical antennas is used, total pattern of the array is then the product of the array factor and the individual element pattern [5]. The array factor of an array is determined by the array arrangement in space, and the amplitude and phase of the feeding currents. Thus, by controlling these variables the response of antenna arrays in any direction can be controlled. Here, this will be shown by examining the uniform linear arrays. A typical structure of linear array is shown in Figure 2.2. The output of each element can be controlled in amplitude and phase as indicated by attenuators and phase shifters in Figure 2.2.

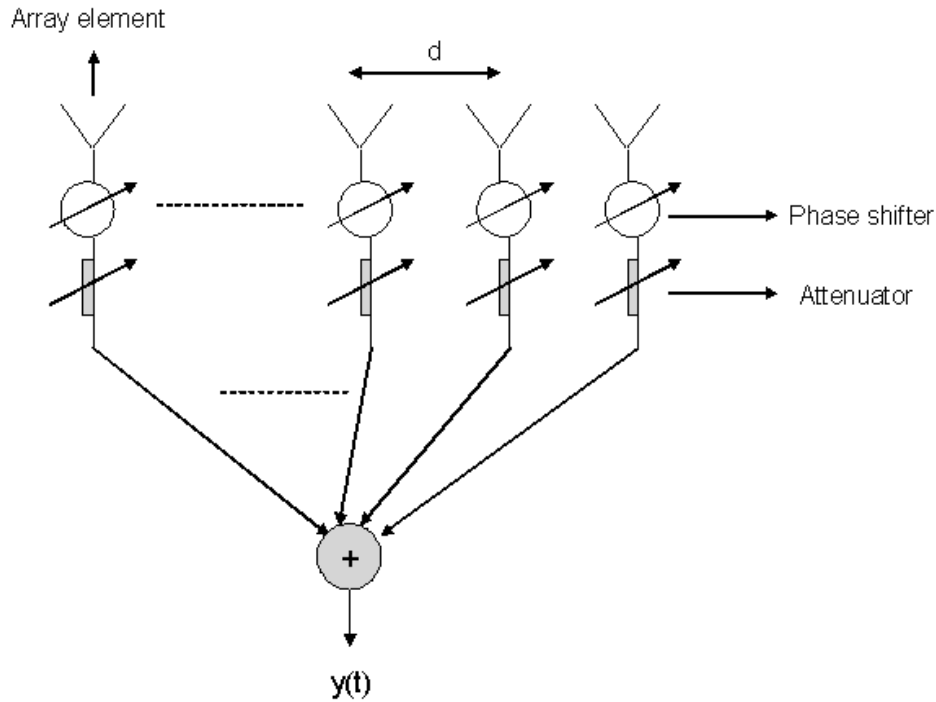


Figure 2.2: Typical linear array structure.

Figure 2.2 can be simplified more, if the attenuators and phase shifters are replaced by the complex weights as shown in Figure 2.3. In Figure 2.3,  $x_i(k)$  is the  $k$ th sample of the complex envelope of signal at the  $i$ th sensor, and  $w_i$  is the complex weight of that branch. Then, the array output of an  $L$  element ULA can be

calculated as :

$$y(k) = \sum_{i=1}^L w_i^* x_i(k) \quad (2.1)$$

where \* denotes complex conjugate.  $x_i(t)$ 's and  $w_i$ 's may be expressed as column vectors,

$$\mathbf{w} = \begin{bmatrix} w_1 \\ \vdots \\ w_K \\ \vdots \\ w_L \end{bmatrix} \quad (2.2)$$

and

$$\mathbf{x}(\mathbf{k}) = \begin{bmatrix} x_1(k) \\ \vdots \\ x_K(k) \\ \vdots \\ x_L(k) \end{bmatrix} \quad (2.3)$$

. The vector  $\mathbf{w}$  is called the complex weight vector and the vector  $\mathbf{x}(\mathbf{k})$  is called array input data vector. Then, Equation 2.1 can be written in matrix form as

$$y(k) = \mathbf{w}^H \mathbf{x}(\mathbf{k}), \quad (2.4)$$

and H denotes the Hermitian transpose. Before continuing to find  $\mathbf{x}(t)$ , assume a plane wave reaches the array from a direction  $\theta$  with carrier frequency  $f_c$ . The angle  $\theta$  called the direction-of-arrival(DOA) of the received signal, and is measured as shown in Figure 2.3. At the first element of the array, complex envelope of the received signal can be represented by the equation below,

$$x_1(t) = a(t)e^{j2\pi f_c t + \psi(t)} + n_1(t). \quad (2.5)$$

where  $a(t)$ , is the amplitude of the signal,  $\psi$  includes digital information.  $n_1(t)$  is the complex envelope of the noise. As shown in Figure 2.3, wavefronts does not reach all of the array elements at the same time, and there exists a path difference between the first and second element. Thus, a phase shift  $e^{-j2\pi\Delta d/\lambda}$  appears between them.

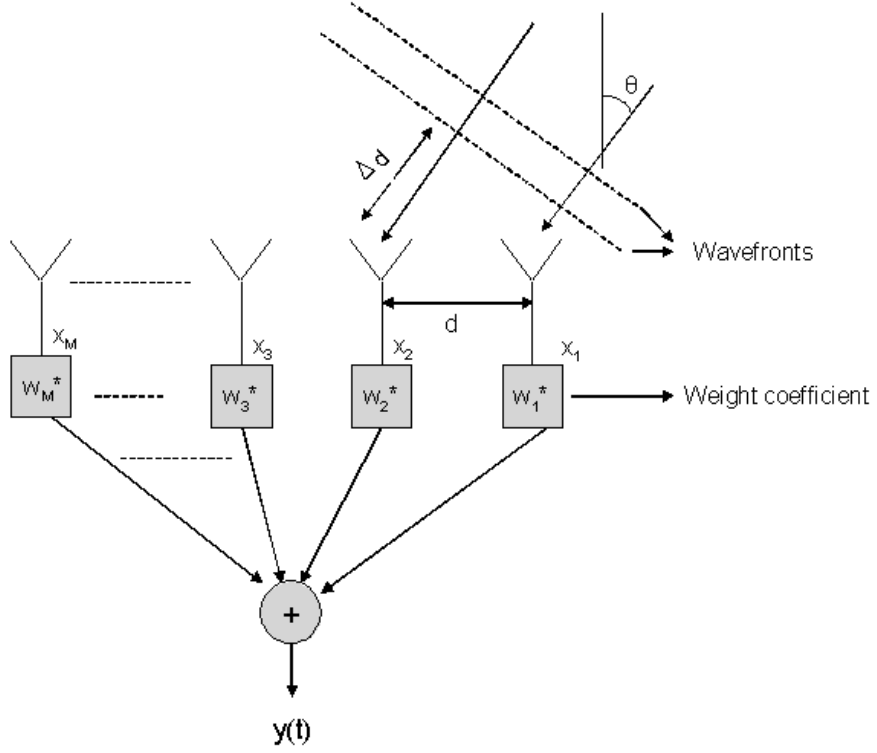


Figure 2.3: A plane wave incident on a ULA from direction  $\theta$ .

As a result, continuing in the same way, complex envelope of the signal at any array element  $K$ , can be expressed in terms of the first element,

$$x_k(t) = x_1(t)e^{-j\frac{2\pi}{\lambda}(K-1)d\sin\theta} + n_k(t). \quad (2.6)$$

where  $\lambda$  is the free-space wavelength of the carrier. Then, Equation 2.3 can be rewritten as

$$\mathbf{x}(t) = \mathbf{s}(\theta)x_1(t) + \mathbf{n}(t). \quad (2.7)$$

where  $\mathbf{n}(t)$  is the noise vector containing the noise samples of the array elements, and  $\mathbf{s}(\theta)$  is called the steering vector and given by the following equation,

$$\mathbf{s}(\theta) = \begin{bmatrix} 1 \\ \vdots \\ e^{-j\frac{2\pi}{\lambda}(K-1)d\sin\theta} \\ \vdots \\ e^{-j\frac{2\pi}{\lambda}(L-1)d\sin\theta} \end{bmatrix} \quad (2.8)$$

Substituting Equation 2.7 to Equation 2.4, we get the following equation

$$y(k) = \mathbf{w}^H \mathbf{s}(\theta)x_1(t) + \bar{\mathbf{n}}(t). \quad (2.9)$$

The first two term in the equation determines the response of the array to signal coming from the direction  $\theta$ , and named as array response that is expressed as in the following equation,

$$r(\theta) = \mathbf{w}^H \mathbf{s}(\theta). \quad (2.10)$$

As seen from the Equation 2.10, the response of the array,  $r(\theta)$ , in any direction  $\theta$  can be controlled by adjusting the weight vector,  $\mathbf{w}$ , in an appropriate way. This is the idea behind the beamformers. Controlling the weights, the pattern of the antenna array can be steered to location where the desired user takes place. Consequently, antenna gain in that direction is increased, while in other directions decreased and that results in increased signal quality for the desired user. Thus, a beamformers (BF) behaves like a directional filter. There are two types of beamformers, narrowband beamformer and wideband beamformer. The scheme in the Figure 2.3 is a narrowband beamformer structure. A wideband beamformer structure is shown in Figure 2.4. A wideband beamformer uses more than one array input vector sample, and in Figure 2.4  $K$  sample is used.

The directional discrimination capability of a beamformer depends on the ratio of  $\frac{d}{\lambda}$  where  $d$  is the distance between the array elements. As the ratio increases discrimination improves [2], as shown in Figure 2.5. However, increasing  $\frac{d}{\lambda}$  results in higher array size and for spacings larger than a half wavelength there may be more than one major lobe [2]. Additional major lobes called grating lobes and in most situations it is undesirable. As a result, generally ULA antennas are separated by a half wavelength.

There are basically two types of beamforming which are being investigated by independent or cellular companies to enhance the performance of their systems namely, switched-beam and adaptive array types.

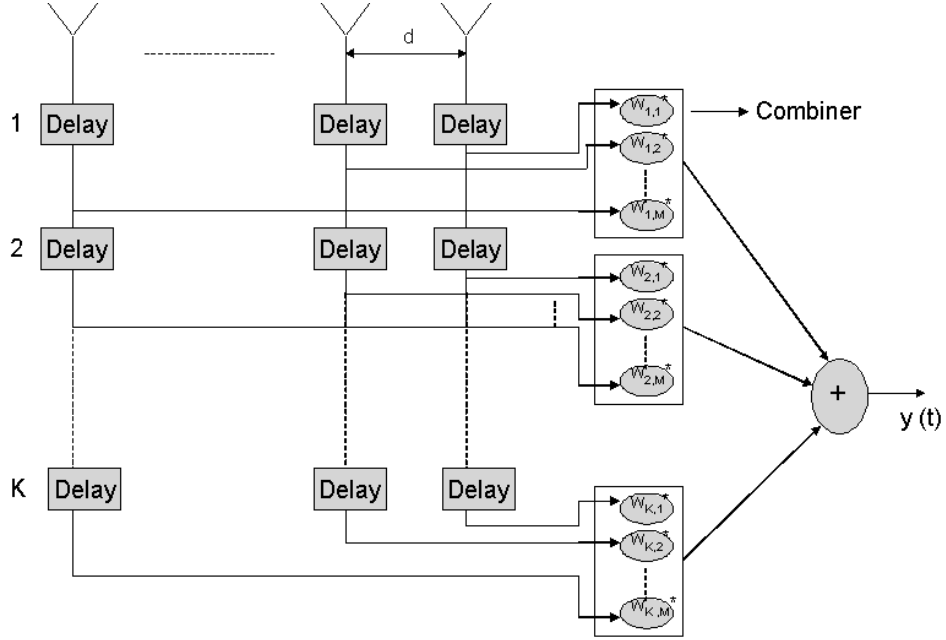


Figure 2.4: A wide band beamformer.

### 2.0.1 Switched-beam Systems

A switched-beam system consists of generating a multiplicity of adjacent beams whose output may be switched to receiver or a bank of receivers [7]. The cell is therefore covered with a cluster of contiguous beams.

The most popular network to form the beams in switched-beam technology is the Butler matrix. The topology of the Butler beam-forming for an eight contiguous beam system is shown in Figure 2.6. There are eight input ports and eight output ports ( $N=8$ ). The matrix consists of quad hybrids, or directional couplers and fixed phase shifters. The amount of each depends on the number of beams generated. For example, for a linear array of  $L$  elements, the number of couplers is

$$n = \left(\frac{L}{2}\right) \log_2 L \quad (2.11)$$

where  $N$  is the number of beams, and the number of phase shifters is

$$n = \left(\frac{L}{2}\right) (\log_2 L - 1) \quad (2.12)$$

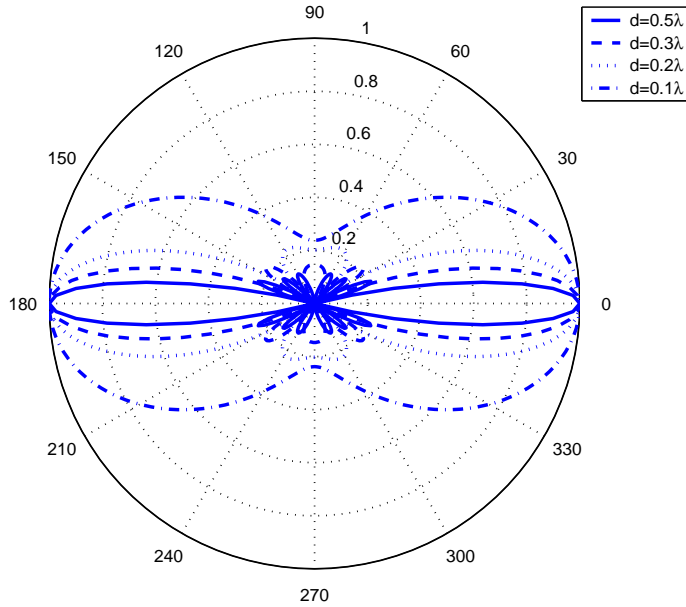


Figure 2.5: Beampatterns for an equal-weight, 8 element ULA beamformer for different  $\frac{d}{\lambda}$ .

Butler arrays can be built to have any power of two beams : 2, 4, 8, 16, 32, and so forth. The number of beams is equal to the number of array elements. The beams are equally spaced and the peaks are located at the nulls of the other beams.

Since the Butler array is uniformly illuminated, this gives the smallest beamwidth possible and maximum gain. This follows from array theory.

For a practical array operating at about 3 GHz, the gain is about 11 dB for the center beams.

## 2.0.2 Adaptive Arrays

The location of a mobile user may change continuously, and that requires the change of array weights continuously for real-time tracking. If the weights are allowed to vary in time, the array becomes an adaptive array. Therefore an adaptive array can dynamically modify its antenna pattern structure to place a directional

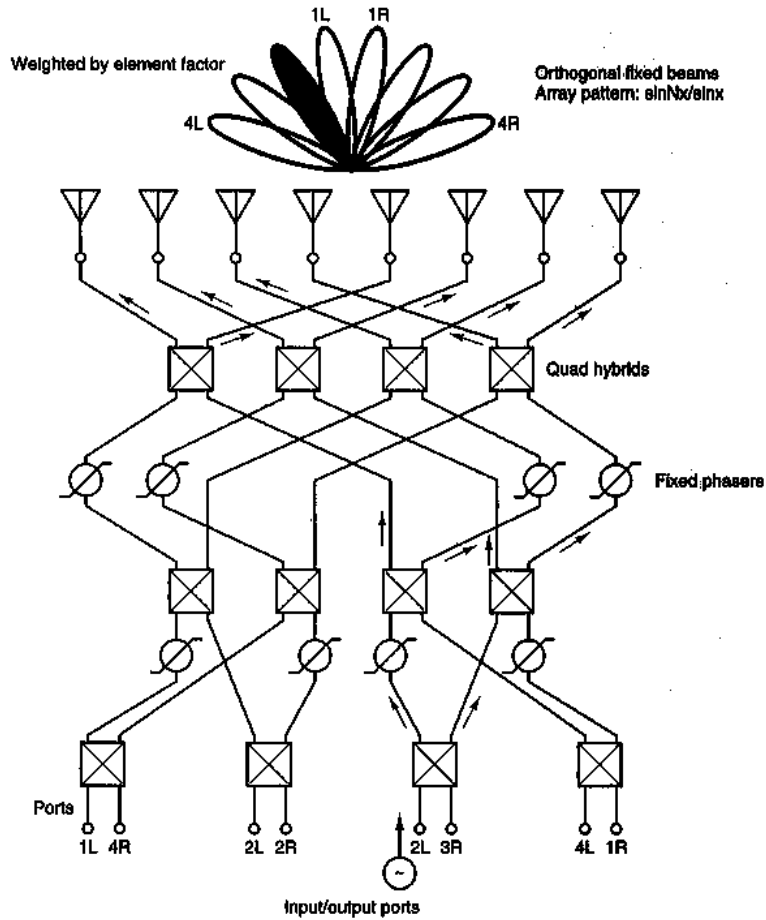


Figure 2.6: A Butler matrix.

beam in the direction of SOI and nulls in the direction of interferers. Typically this would be done by means of an internal feedback control and estimating the desired weights using a digital signal processor (DSP) as shown in Figure 2.7 .

If a base station in a cellular system uses an adaptive array to direct its radiation pattern towards the mobile which it is communicating, then several benefits are produced.

- The transmit power for a given signal quality can be reduced in both uplink and downlink directions, or the cell radius can be increased, thereby reducing the number of base stations required to cover a given area.

- Since the mobile transmit power is reduced, its battery life can be extended.
- The channel delay spread is reduced since off-axis scatters are no longer illuminated.
- Depending on the direction of the mobile, the probability of base stations causing interference to co-channel mobiles in surrounding cell is reduced.
- Similarly, the probability of mobiles causing interference to co-channel base station is reduced.

This last point is known as spatial filtering for interference reduction (SFIR). The average level of interference between co-channel cells is reduced so the reuse distance  $D$  can be decreased, thereby increasing the system capacity. Notice that the interference reduction is statistical, the level of interference will depend on the positions of the mobiles in each cell at any time.

Most adaptive algorithms determines the weights by optimizing some measure of the system performance [8], such as signal-to-interference-and-noise ratio(SINR), minimum noise variance, minimum output power.

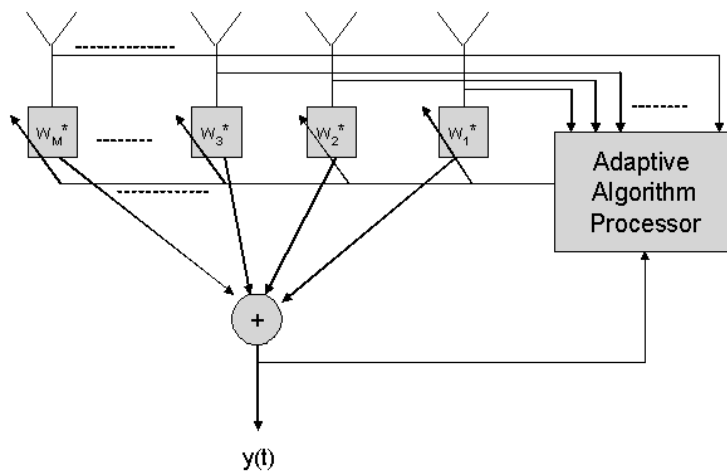


Figure 2.7: Adaptive array.

There will be a detailed discussion about the adaptive array algorithms in the next section.

## 2.1 Smart Antenna Algorithms

There are several algorithms for adaptive arrays, or Smart Antennas (SA), presented in literature. According to the side information used for beamforming, the algorithms can roughly be divided into three groups [9].

- Algorithms based on DOA estimation of the incoming signal, direction of arrival based beamformer (DOB) .
- Algorithms exploiting a training sequence, which can be considered as a temporal reference beamformer (TRB).
- Algorithms based on signal structure, signal-structure-based beamformer (SSBF).

SSBF exploits the temporal and/or spectral properties of the received signals such as finite alphabet structures of digital signals or constant modulus property of PSK signals. In the mobile scenario, a DOB requires AOA tracking. Since TRB uses a training signal, spectral efficiency is reduced.

### 2.1.1 Direction of Arrival-Based Beamforming

In the DOB, the DOAs of the received signals are determined first using DOA estimation techniques, then the beamformer (BF) weights are calculated. There are three main types of optimum BF's: BF's based on signal-to-interference-plus noise ration (SINR) maximization, maximum likelihood (ML) and minimum variance distortionless response (MVDR). Another group of DOB's is data-independent BF's, conventional beamformer (CBF) and null-steering beamformer. DOB techniques analytically more tractable, but these methods needs calibration. Also, DOA estimation requires that the number of signals incident on the array should be less than the number of antenna elements. DOB performance can be seriously degraded

in the presence of coherent multipath, producing signal cancellation at the array output.

A conventional beamformer is the simplest beamformer. If a desired signal from a known DOA is chosen, then the main beam can be steered towards this direction by simply multiplying each element by a complex weight, corresponding to a delay, so that when the signals are combined the signals from the desired direction at each element add completely in phase. With  $\mathbf{s}_0$  denoting the steering vector in the desired direction, the array weights are given by

$$\mathbf{w} = \frac{1}{L} \mathbf{s}_0 \quad (2.13)$$

where  $L$  is the number of array elements. In an environment consisting of only uncorrelated noise and no directional interferences, this beamformer provides maximum SNR. For uncorrelated noise, the noise power at the array output is  $L$  times less than that present on each element.

The limiting factor in the performance of this method is that it has no control over its side lobes, where the antenna pattern allows the interfering signal to reach the receiver after the weights are applied. The null steering beamformer adapts the weight vector to steer the main beam towards the desired signal and place nulls in the direction of interfering user. Assume that  $\mathbf{s}_0$  is the steering vector in the direction of desired signal and that  $\mathbf{s}_1, \dots, \mathbf{s}_k$ , are  $k$  steering vectors in the direction of interferers, desired weight vector is the solution of following equations.

$$\begin{aligned} \mathbf{w}^H \mathbf{s}_0 &= 1 \\ \mathbf{w}^H \mathbf{s}_i &= 0, i = 1, \dots, k \end{aligned} \quad (2.14)$$

Using matrix notation, this becomes

$$\mathbf{w}^H \mathbf{S} = \mathbf{e}_1^T. \quad (2.15)$$

where  $\mathbf{S}$  is the matrix of steering vectors and  $\mathbf{e}_1$  is a vector of all zeros except the first element is one, that is

$$\mathbf{S} = [\mathbf{s}_0, \mathbf{s}_1, \dots, \mathbf{s}_k] \quad (2.16)$$

$$\mathbf{e}_1 = [1, 0, \dots, 0]^T. \quad (2.17)$$

the solution for the weight vector is given by

$$\mathbf{w}^H = \mathbf{e}_1^T \mathbf{S}^{-1}. \quad (2.18)$$

The null-steering scheme described above requires knowledge of the directions of interference sources, and the BF using the weights estimated by this scheme does not maximize the output SINR. Optimum DOB's overcome this limitation.

Let  $\mathbf{w}$  represent the weights of the BF, which maximizes the output SINR. For an array that is not constrained, an expression for  $\mathbf{w}$  is given by

$$\mathbf{w} = \mu_0 \mathbf{R}_N^{-1} \mathbf{s}_0. \quad (2.19)$$

where  $\mathbf{R}_N$  is the array correlation matrix of the interference plus noise alone, that is, it does not contain any signal arriving from the look direction  $(\phi_0, \theta_0)$ , and  $\mu_0$  is a constant. For an array constrained to have a unit response in the look direction, this constant becomes

$$\mu_0 = \frac{1}{\mathbf{s}_0^H \mathbf{R}_N^{-1} \mathbf{s}_0}. \quad (2.20)$$

then the weight vector becomes

$$\mathbf{w} = \frac{\mathbf{R}_N^{-1} \mathbf{s}_0}{\mathbf{s}_0^H \mathbf{R}_N^{-1} \mathbf{s}_0} \quad (2.21)$$

This is also known as ML filter [10], as it finds the ML estimate of the power of the signal source, assuming all sources as interferences.

In practice, when the estimate of the interference-plus-noise- alone matrix is not available, the total R (signal + interference + noise), array correlation matrix, is used to estimate the weights. In this case, the weight vector calculated as,

$$\mathbf{w} = \frac{\mathbf{R}^{-1} \mathbf{s}_0}{\mathbf{s}_0^H \mathbf{R}^{-1} \mathbf{s}_0} \quad (2.22)$$

These weights are the solution of the following optimization problem :

$$\min_{\mathbf{w}} (\mathbf{w}^H \mathbf{R} \mathbf{w}) \quad \text{subject to} \quad \mathbf{w}^H \mathbf{s}_0 = 1 \quad (2.23)$$

The constraint ensures that the signal passes through the processor undistorted. The minimization process then minimizes the total noise, including interferences and uncorrelated noise. Therefore this algorithm is also known as Minimum Variance Distorsionless Response (MVDR).

MVDR minimizes the total output power while keeping the output signal constant, it is the same as maximizing the output SINR. Therefore, it can be proved that the weights of ML filter and MVDR, equation 2.21 and 2.22, are identical [11].

DOA estimation is an important part of DOB's. The high-resolution techniques for DOA estimation include MUSIC and ESPRIT.

### DOA Estimation Techniques

Spectral estimation methods estimate the DOA by computing the spatial spectrum and then determining the local maximas. One of the earliest methods is the Bartlett method. By steering the array in  $\theta$  direction, this method estimates the mean power, which is given by

$$P_B(\theta) = \frac{\mathbf{s}_0^H \mathbf{R} \mathbf{s}_0}{L^2} \quad (2.24)$$

where  $L$  is the number of array elements. MVDR estimator uses the array weights, which are obtained by minimizing the mean output power subject to unity constraint in the look direction. An expression for the power spectrum is given by

$$P_{MV}(\theta) = \frac{1}{\mathbf{s}_0^H \mathbf{R}^{-1} \mathbf{s}_0} \quad (2.25)$$

This method has better resolution properties than Bartlett method.

One of the other methods for DOA estimation, having good resolution properties, is eigenstructure methods. These methods rely on the following properties of  $\mathbf{R}$ : 1) The space spanned by its eigenvectors may be partitioned into two subspaces, namely the signal subspace and the noise subspace, and 2) the steering vectors corresponding to the directional sources are orthogonal to noise subspace. As the noise subspace is orthogonal to the signal space, these steering vectors are contained

in the signal subspace. The noise subspace is spanned by the eigenvectors associated with the smaller eigenvalues of the correlation matrix, and the signal subspace is spanned by the eigenvectors associated with its larger eigenvalues [11].

In principle, the eigenstructure-based methods search for the directions such that the steering vectors associated with these directions orthogonal to the noise subspace and are contained in the signal subspace. In practice, first find a weight vector that is contained in the noise subspace, then search for the directions such that the associated steering vectors are orthogonal to this vector. Two of the most important eigenstructure methods are Multiple Signal Classification algorithm (MUSIC) [12], and Estimation of Signal Parameters via Rotational Invariance Technique (ESPRIT) [13].

Spectral MUSIC estimates the noise subspace from the available samples. This can be done by either eigenvalue decomposition of the estimated array correlation matrix.

In a  $L$  element antenna array, once the noise subspace has been estimated, DOA for  $D$  directions is estimated by searching for peaks in the MUSIC spectrum given by

$$P_{MUSIC}(\theta) = \frac{1}{|\mathbf{s}_\theta^H \mathbf{U}_N|^2} \quad (2.26)$$

where  $\mathbf{U}_N$  is a matrix and its columns are the eigenvectors corresponding to the  $L-D$  smallest eigenvalues of the array correlation matrix, and  $\mathbf{s}_\theta$  denotes the steering vector corresponding to direction  $\theta$ .

The advantage of this algorithm is that it exhibits high resolution. However, it can be computationally intensive, since it requires a search through the entire array manifold for the steering vectors that are orthogonal to noise subspace. Furthermore, the MUSIC works on the premise that the signals impinging on the array are not fully correlated. The performance of MUSIC degrades severely in a highly correlated signal environment as encountered in multipath propagation. This problem is solved

by modification of covariance matrix through a processing scheme called spatial smoothing [14].

Other types of MUSIC are Root-MUSIC and Cyclic-MUSIC algorithms [15]. The Root-MUSIC applicable when a ULA is used. It solves a polynomial rooting problem, the poles of  $P_{MUSIC}(\theta)$ , in contrast to the identification and localization of spectral peaks using MUSIC. Root-MUSIC has a better performance than spectral MUSIC. Cyclic MUSIC computes the cyclic autocorrelation matrix  $\mathbf{R}_{xx}^\alpha$  of the array input data vector  $\mathbf{x}(t)$ , since only the desired signals exhibit spectral correlation at a particular frequency  $\alpha$ . Then works in a similar way to spectral-MUSIC.

ESPRIT is a computationally efficient and robust method of DOA estimation [13]. It uses two identical arrays. Second array,  $\mathbf{y}$ , is obtained by shifting the each element of the first array,  $\mathbf{x}$ , by the same displacement vector,  $\Delta_0$ , to form matched pairs. The working principle of ESPRIT based on that, the matrices  $\mathbf{U}_x$  and  $\mathbf{U}_y$  respectively, containing the eigenvectors of two array correlation matrixes  $\mathbf{R}_{xx}$  and  $\mathbf{R}_{yy}$  in its columns, related by the transformation matrix  $\psi$

$$\mathbf{U}_x \psi = \mathbf{U}_y \quad (2.27)$$

and the eigenvalues of  $\psi$  are equal to

$$\Phi_l = e^{2\pi\Delta_0\cos\theta_l} \quad (2.28)$$

where  $\theta_l$  is the direction of the incoming signal  $l$ . An eigendecomposition of  $\psi$  gives its eigenvalues,  $\lambda_l$  and by equating them to  $\Phi_l$  leads to the DOA estimates

$$\theta_l = \cos^{-1}\left\{\frac{\text{Arg}(\lambda_l)}{2\pi\Delta_0}\right\}, \quad l = 1, \dots, L. \quad (2.29)$$

How one obtains an estimate of  $\psi$  from the array signal measurements has led to many versions of ESPRIT. This class of algorithms also provides the high resolution of MUSIC, but it does not require a costly search. The ESPRIT algorithm allows the DOAs to be computed directly, and has been used with different array geometries.

How one obtains an estimate of  $\psi$  from the array signal measurements has led to many versions of ESPRIT. This class of algorithms also provides the high resolution of MUSIC, but it does not require a costly search. The ESPRIT algorithm allows the DOAs to be computed directly, and has been used with different array geometries.

Maximum Likelihood (ML) method estimates the DOA's from a given set of array samples by maximizing the log-likelihood function that tries to find the best fit with the received array inputs and the array response . Since ML techniques were computationally intensive, they were less popular than subspace based techniques. However, in terms of performance, the ML techniques are superior to the subspace techniques , especially in low SNR conditions. Moreover, unlike subspace based techniques, ML based techniques can also perform well in correlated signal conditions [16].

### **2.1.2 Temporal Reference-Based Beamforming (TRB)**

Beamforming based on training signal or time reference beamforming is a computationally effective method at the expense of spectrum efficiency. Spatial information such as an DOA or array manifold are not necessary. The reference signal may consist of an a priori known signal or reconstructed signal obtained from the detected symbols. The use of training signals requires prior carrier and signal recovery, which is difficult due to the presence of co-channel interference (CCI).

The adaptive algorithms Least-Mean-Squares (LMS) and Recursive-Least-Squares (RLS), are used for tracking and discussed in [11]. The TRB overcomes interference by nulling its spatial signatures and shows greater robustness in the mobile environment where the channel characteristics are continuously varying. The TRB technique optimally combines multipath components to increase SNR and reduce the effect of fading.

In a noncoherent multipath environment, both the DOB and TRB have the

same ability to overcome ISI since two different symbols for the same user will be uncorrelated and will look like noise[9].

Instead of calibration in the DOB, the TRB technique require accurate synchronization.

TRB is based on Wiener solution, which gives the optimum weights that minimizes mean-squared error(MSE) between the reference signal samples,  $r(t)$ , and the array output samples,  $y(k)$ . Optimum weight, found according to Wiener solution, is given by,

$$MSE = E[|y(k) - r(k)|^2] \quad (2.30)$$

$$\mathbf{w}_{MSE} = \mathbf{R}^{-1}\mathbf{z}. \quad (2.31)$$

where  $\mathbf{R}$  is the array correlation matrix,  $R = E[xx^H]$ , and  $\mathbf{z}$  is the cross-corelation between  $r^*$  and array input vector  $\mathbf{x}$ ,  $\mathbf{z} = E[r^*\mathbf{x}]$ . In practice, neither  $\mathbf{R}$  nor  $\mathbf{z}$  is available to calculate the optimal weights of the array, and the weights are adjusted using the available information derived from the array output.

Least Mean Squares (**LMS**) algorithm updates the weights at each iteration by estimating the gradient of the mean-square error,  $g$ , and then moving the weights in the negative direction of the gradient by a small amount, determined by the constant step size  $\mu$ ,

$$\mathbf{w}(k+1) = \mathbf{w}(k) - \mu g(w(k)) \quad (2.32)$$

The instantaneous estimate of gradient is computed as in the following equation, [11],

$$g = 2\mathbf{x}(k)e^*(k) \quad (2.33)$$

Substituting Equation 2.33 into Equation 2.32, we get the weights in the LMS algorithm ,

$$\mathbf{w}(k+1) = \mathbf{w}(k) - 2\mu\mathbf{x}(k)e^*(k) \quad (2.34)$$

where  $e$  is the error signal,  $e=y(k)-r(k)$ .

LMS algorithm is easy to implement, however its convergence and stability characteristics is strictly dependent on the eigenvalues of  $\mathbf{R}$ . For  $\mu < 1/\lambda_{max}$ , with  $\lambda_{max}$

denoting the maximum eigenvalue of  $\mathbf{R}$ , the algorithm is stable and the mean value of the estimated weights converges to the optimal weights. The convergence speed of the algorithm is characterized by the eigenvalue spread of the  $\mathbf{R}$  matrix. The larger the eigenvalue spread, the longer it takes for the algorithm to converge.

Normalized LMS algorithm is a variation of the constant-step-size LMS algorithm and uses a data-dependent step size at each iteration. At the  $n$ th iteration the step size is given by

$$\mu(n) = \frac{\mu_0}{\mathbf{x}^H(n)\mathbf{x}(n)} \quad (2.35)$$

where  $\mu_0$  is a constant. It avoids the need for estimating the eigenvalues of the correlation matrix for the selection of the maximum step size. The algorithm has better convergence performance compared to the normal LMS algorithm [17].

The convergence speed of the LMS algorithm depends on the eigenvalues of  $\mathbf{R}$ . **RLS**, [18], solves this problem by replacing step size  $\mu$  in LMS algorithm with a gain matrix  $\mathbf{R}^{-1}(k)$  at the  $k$ th iteration, producing the weight update equation,

$$\mathbf{w}(k) = \mathbf{w}(k-1) - \mathbf{R}^{-1}(k)\mathbf{x}(k)e^*(k) \quad (2.36)$$

The RLS algorithm updates the required inverse of  $\mathbf{R}(n)$  using the previous inverse and the present sample as

$$\mathbf{R}^{-1}(k) = \frac{1}{\delta_0} \left[ \mathbf{R}^{-1}(k-1) - \frac{\mathbf{R}^{-1}(k-1)\mathbf{x}(k)\mathbf{x}^H(k)\mathbf{R}^{-1}(k-1)}{\delta_0 + \mathbf{x}^H(k)\mathbf{R}^{-1}(k-1)\mathbf{x}(k)} \right] \quad (2.37)$$

where  $\delta_0$ , a real scalar smaller than but close to one, is used for exponential weighting of the past data and de-emphasize the old samples.

The RLS algorithm minimizes the cumulative square error [15]

$$J(k) = \sum_{n=0}^k \delta_0^{k-n} |e(n)|^2 \quad (2.38)$$

and its convergence is independent of the eigenvalue distribution of the correlation matrix. The resulting rate of convergence is faster than the simple LMS algorithm.

### 2.1.3 Signal-Structure Based Beamforming (SSBF)

In signal-structure-based beamforming, adaptive processors exploit temporal and/or spectral structures and properties of the received signal to compute the

weight vector,  $w$ . Many SSBF's try to restore the signal property, for example, a constant modulus(CM) for several modulation schemes or finite alphabet property of digital signals. This blind BF method is very robust against different propagation conditions, but its convergence and capture characteristics can be problematic.

**Constant Modulus Algorithm** (CMA) is a gradient-based algorithm that works on the premise that the existence of interference causes fluctuation in the amplitude of the array output, which otherwise has a constant modulus. Phase-shift keying (PSK ), frequency-shift keying (FSK) signals have this constant modulus property. In CMA, the weights are updated by minimizing the MSE cost function [19]

$$MSE = E[|y(k)|^p - |\alpha|^p|^q]. \quad (2.39)$$

where  $\alpha$  is the desired signal amplitude at the array output. The exponents  $p$  and  $q$  are each equal to either 1 or 2. Using different values of  $p$  and  $q$  , it is possible to develop several different algorithms which have different characteristics. In [3], for  $p = 1, q = 2$  form, using the instantaneous estimate of the gradient vector of Equation 2.39 the following algorithm is obtained,

$$\mathbf{w}(k+1) = \mathbf{w}(k) - \mu \mathbf{x}(k) e^*(k) \quad (2.40)$$

where  $e$  is

$$e(k) = (y(k) - \frac{y(k)}{|y(k)|}) \quad (2.41)$$

Also in [11], for  $p = 2, q = 2$  form, using the same gradient method, a different algorithm is reached,

$$\mathbf{w}(k+1) = \mathbf{w}(k) - 2\mu \mathbf{x}(k) e(k) \quad (2.42)$$

where  $e$  is

$$e(k) = (|y(k)|^2 - 1)y(k) \quad (2.43)$$

CM type of algorithms simply captures the strongest constant envelope signal present at the input, which may be an interfering signal. It has been shown that CMA converges under a wide range of conditions.

Another approach is that, instead of iterating weights using input vectors one by one, block by block basis can be used for a faster convergence. This method is known as **LS-CMA**, [20], and minimizes the total error over K samples using the cost function

$$J(w) = \sum_{k=1}^K ||y(k)| - 1|^2 = \sum_{k=1}^K ||\mathbf{w}^H \mathbf{x}(k)| - 1|^2 \quad (2.44)$$

In [3], the weight, minimizing the cost function above, is found as follows,

$$\mathbf{w} = [\mathbf{X} \mathbf{X}^H]^{-1} \mathbf{X} \mathbf{r}^*. \quad (2.45)$$

where X denote the input data block, consists of K snapshots of array input vectors and r is the complex-limited output data vector,

$$\mathbf{r} = \left[ \frac{y(1)}{|y(1)|}, \frac{y(2)}{|y(2)|}, \dots, \frac{y(K)}{|y(K)|} \right]^T. \quad (2.46)$$

Since the LS-CMA can utilizes the information in a data block, it converges faster than the gradient-based CMA algorithm.

Other types of SSBF are the algorithms that utilizes the signal constellation of digital modulated signals . At baseband, digital modulated signals can take only limited values on complex plane if there were no noise and this information is used by Iterative Least Squares Projection (**ILSP**) algorithm and Irative least squares with enumeration (**ILSE**) algorithm [21]. Instead of updating the weight vector the idea is to visit the received data iteratively until a best fit with the channel (array response) and finite alphabet of the signal is obtained.

The FA property is stronger than CM for digital signals since the signals are restricted to lie on the discrete points in a disk.

The ILSP algorithm performs well with no prior estimate of the array responses, and can be used to initialize ILSE. For a sufficiently good initialization ILSE algorithm converges rapidly to the ML estimate of the array responses and signal symbol sequences [21]. However these algorithms have two impotent deficiency, the number of signal impinging on the array is required and they must be synchronous.

## 2.2 Implementation Aspects of Smart Antenna Systems

Generally all signal processing in the adaptive array antenna are performed in the baseband since the adaptive algorithms require the input vector. Then, it is required to have the same number of frequency converters and analog-to-digital converters as the number of array elements to perform baseband signal processing. It will lead to more occupied area, higher weight and costs than omnidirectional antennas. Furthermore, a DSP or application specific integrated circuits (ASICs) calculates and applies weights to baseband samples. However, current DSP technology has a speed bottleneck in data I/O.

Another difficulty is mutual coupling. Due to mutual coupling between array elements the actual response of the antenna array can deviate significantly.

Recently, researchers have focused on the problems above for practical implementation of smart antennas. To relieve the DSP I/O congestion, in [22] a novel smart antenna system is proposed based on analog beamformer at IF (intermediate frequency) stage. In [23], a novel algorithm is proposed to reduce the receiver chains in a smart antenna system. In [24], [25], methods to compensate the mutual coupling effects, experimental results and simulation results can be found.

# Chapter 3

## Smart Antenna Algorithms Used in CDMA system

### 3.1 Introduction

The increasing demand for mobile communication services entails new techniques to improve spectrum utilization. The Code Division Multiple Access (CDMA) and smart antennas are two promising approaches to increase the system capacity and spectrum efficiency for mobile communication services [15].

The 3<sup>rd</sup> generation (3G) systems are based on wideband CDMA (W-CDMA) technology. The 3G systems will have to handle multi-rate mixed traffic, comprising not only plain noise users, but also the high-rate multimedia users. To maintain acceptable system capacity and network performance, tight power control must be carried out both for the data users and for the voice users since a serious power imbalance between high and low data rate users may exist. However tight power control is not only expensive but also difficult to achieve. Furthermore, power control alone cannot address the issue of power imbalance between high rate and low rate users.

The above problems in 3G systems can be effectively tackled by using smart antennas. Since there are normally only a few high rate users but many low rate users, nulls can be directed towards the high data rate users, as a result, the signal quality for the low data rate users will be greatly improved. Alternatively, more can be accommodated in the same network. On the other hand, main beams can also

be directed towards high data rate users to reduce the interference from the mass of low data rate users. Similarly, high and low data rate users from the same angle can be separated using vertical beamforming. Finally, the accuracy requirement for the overall power control will be relaxed.

## 3.2 W-CDMA

In this section, W-CDMA and W-CDMA uplink will be discussed briefly since in our test-bed only the W-CDMA uplink is used.

W-CDMA is a code-division multiple access technology that separates the user's voice and data information by multiplying pseudo-random bits called "chips". The pseudo-random bit sequences have a chip rate of 3.84 Mcps, resulting the narrow-band information of the user being spread across a wider bandwidth of approximately 5 MHz.

In the spreading process, information symbols are multiplied by a high-rate spreading code consisting of chips as shown in Figure 3.1. The resulting signal has a wider bandwidth dependent on the number of chips per second. In the de-spreading process, the spreading codes is multiplied by the received signal to recover the original data symbols. Spreading codes are specially designed to allow the symbols from multiple users to occupy the same spectrum at the same time, while still allowing the original information to be retrieved.

Key specifications of W-CDMA technology are [1] :

- Multiple access technique : Direct-spread code division multiple access.
- Chip rate of spreading codes : 3.84 Mcps.
- Bandwidth : 4.4 - 5 MHz.
- Duplexing options :Frequency division and time division duplex.
- Multipath reception : Due to wide bandwidth, can resolve multipath signals ,and provides diversity gain

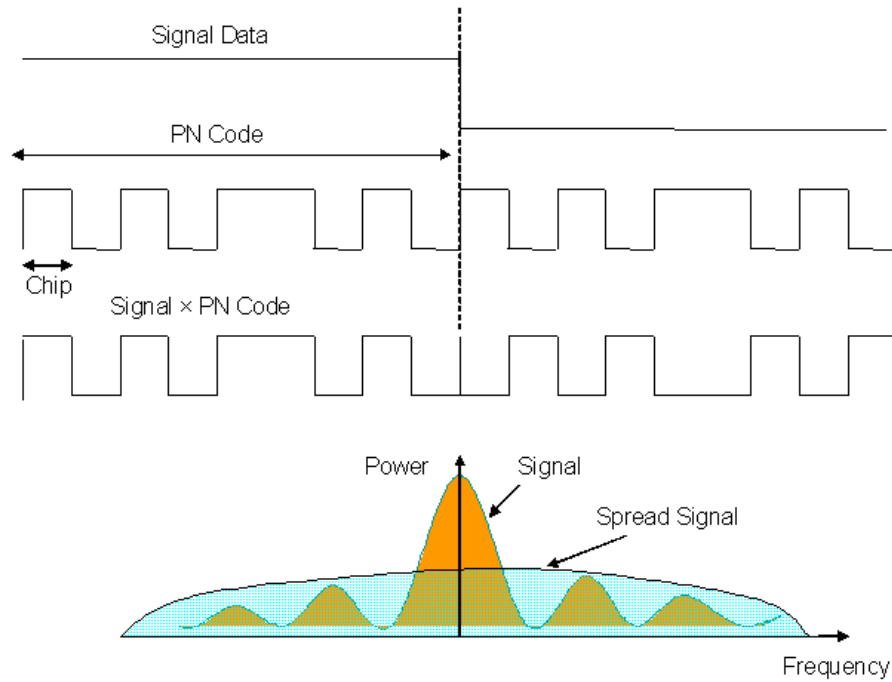


Figure 3.1: W-CDMA spreading and power spectrum.

- Power control : 1500 Hz on both links, to overcome near-far problem.
- Frequency reuse of 1 : Every base station in the CDMA system operates on the same frequency
- Soft capacity : By setting the allowed interference threshold lower, coverage will improve at the expense of capacity. By setting the threshold higher, capacity will increase at the expense of coverage.

W-CDMA defines two dedicated physical channels in both uplink and downlink [1] :

- Dedicated Physical Data Channel (DPDCH) : to carry dedicated data.
- Dedicated Physical Control Channel (DPCCH) : to carry dedicated control information.

Spreading is applied after data modulation in two stages. First, the bipolar data symbols on I and Q channels are independently multiplied by different channelization codes known as Orthogonal Variable Spreading Factor (OVSF) codes. The resultant signal is multiplied by a complex scrambling codes. The complex scrambling code is a unique signature of the mobile station. Next, the scrambled signal is passed through the pulse shaping filter, Square-Root-Raised Cosine filter with roll-off factor of 0.22, that determines the final spectrum properties of the modulation scheme, and then upconverted as shown in Figure 3.3.

The most important purpose of the spreading codes to provide the orthogonality between different physical channels of the uplink user. OVSF codes generated by using the code-tree shown in the Figure 3.2. Each level on the code tree defines spreading codes of length SF(Spreading Factor). All the codes of the same level constitute a set and orthogonal to each other. Any two codes of different levels are orthogonal to each other as long as one of them is not the mother of the other code [1].

The tree-structured OVSF codes at level  $2n$ , as shown in Figure 3.2, are generated using the following equation [1]:

$$C_{2n} = \begin{bmatrix} C_{2n,1} \\ C_{2n,2} \\ \vdots \\ C_{2n,2n} \end{bmatrix} = \begin{bmatrix} C_{n,1} & C_{n,1} \\ C_{n,1} & -C_{n,1} \\ \vdots & \\ C_{n,n} & C_{n,n} \\ C_{n,n} & -C_{n,n} \end{bmatrix} \quad (3.1)$$

### 3.3 Smart Antenna Algorithms for CDMA Systems

In this section SA algorithms, developed for CDMA [3], are presented. Any algorithm developed for CDMA must have the property of separating user's operating at the same frequency and blind algorithms are preferred for further spectral efficiency.

Multitarget Least Squares Constant Modulus Algorithm (MT-LSCMA) [2], Multitarget Decision-Directed (MT-DD) Algorithm [3] are the first two algorithms

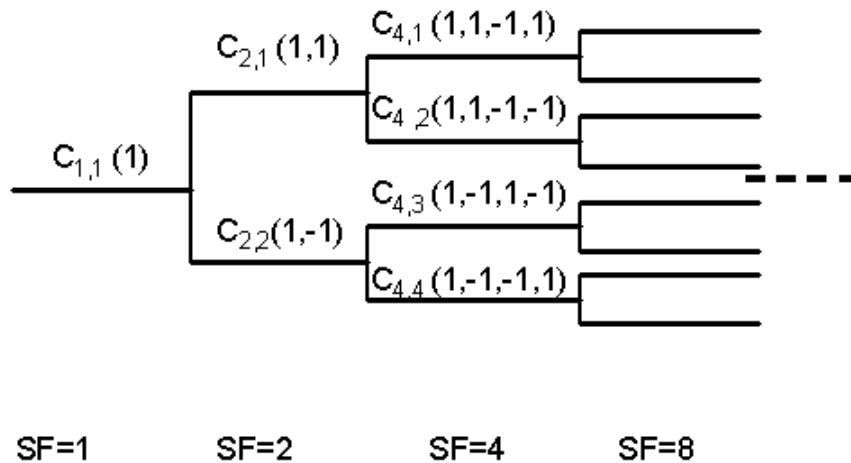


Figure 3.2: Code tree for generation of OVSA codes.

thought to be convenient for CDMA. MT-LSCMA [2], is a multitarget adaptive algorithm using dynamic LS-CMA. CMA is constant modulus based algorithm, exploiting the constant modulus envelope of the CDMA signals, and may yields weight vectors converged to same value. MT-DD algorithm has the same problem, moreover both algorithms have the phase ambiguity problem. In [3], Gram-Schmidt Orthogonalization (GSO) is proposed to prevent the weights from converging to same value. However this method limits the number of output ports and having ensured that weight vectors at each port converges to different values, a sorting procedure must be performed to determine which port belongs to which user. Also phase ambiguity problem must be solved applying appropriate methods as suggested in [3], using DPSK (Differential Phase Shift Keying) or sending pilot signal to compensate the phase rotation.

Least- Squares De-spread Respread Multitarget Array (LS-DRMTA) [3] and Least- Squares De-spread Respread Multitarget Constant Modulus Algorithm (LS-DRMTCMA) [3] are developed by Rappaport and Rong [3]. Both algorithms have neither phase ambiguity problem nor the problem of weight vectors converges to same value and implemented in our test-bed software. In the following subsections they will be discussed in more detail.

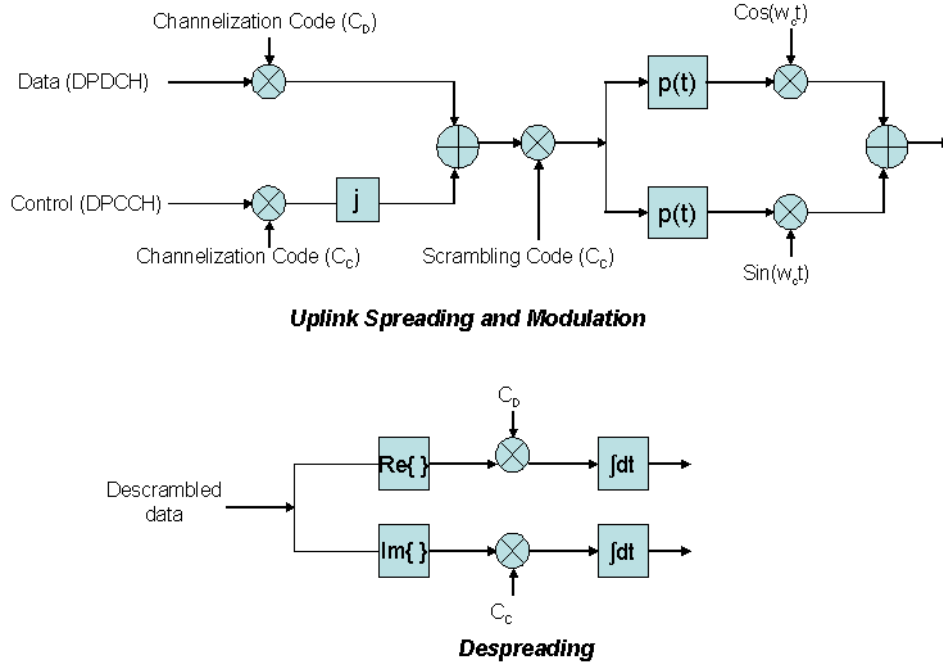


Figure 3.3: Uplink spreading and de-spreading for W-CDMA having carrier frequency  $w_0$ .

### 3.3.1 Least Squares De-spread Re-spread Multitarget Array

Neither MT-DD nor MT-LSCMA utilizes the user specific spreading signals that is known by the base station in a CDMA system. However this information can be used for an efficient BF. LS-DRMTA is such an algorithm that utilizes spreading signals. Utilizing the user's spreading signal renders LS-DRMTA more advantageous than MT-LSCMA and MT-DD algorithm. In LS-DRMTA each user's weight vector is found by minimizing a cost function special to that user, since the cost function in Equation 3.2 is directly related to the user's spreading signal. This property circumvents it from the necessity of performing GSO and sorting procedures, that causes increased complexity and limits the number of output ports by the number of array elements in MT-DD and MT-LSCMA. As a result LS-DRMTA has a lower computational complexity with respect to MT-DD and MT-LSCMA, and the number of output ports can be greater than the number of array elements. Figure 3.4 demonstrates the structure of a BF using LS-DRMTA algorithm.

LS-DRMTA block diagram is shown in Figure 3.5, after a bit detection, it is respread again to obtain the received signal. LS-DRMTCMA works on the premise that, if the bit is detected correctly, then received signal and respread signal must be similar to each other. As a result in [3], this information is used to generate the BF weights and LS-DRMTA tries to minimize the cumulative square error over K samples of array output,  $y_i(t)$ , and re-spread signal,  $r_i(t)$

$$\begin{aligned}
 J(\mathbf{w}) &= \sum_{k=1}^K |y_i(k) - r_i(k)|^2 \\
 &= \sum_{k=1}^K |\mathbf{w}_i^H \mathbf{x}(k) - r_i(k)|^2
 \end{aligned} \tag{3.2}$$

and 3.2 leads to least squares solution and the weight vector in the  $l^{th}$  iteration can be found as,

$$\mathbf{w}(l+1) = [\mathbf{X} \mathbf{X}^H]^{-1} \mathbf{X} \mathbf{r}_i^* \tag{3.3}$$

where X is a matrix containing K snapshot of array input data vector in each column. If the iteration is done after each bit detection, K will be equal to the number of samples per bit.

For any user i, the algorithm is implemented as follows. First using the block of array input data snapshots the matrix X is generated. The array output is despread and the bit is detected, then it is spread again by the PN sequence belongs that user to obtain  $r_i(t)$ . Finally using  $r_i(t)$  and X, the weights are adjusted according to Equation 3.3 until the algorithm converges.

### 3.3.2 Least Squares De-spread Re-spread Multitarget Constant Modulus Algorithm

Similarly, LS-DRMTCMA utilizes the spreading signal of each user like LS-DRMTA, so it possesses all the advantages of LS-DRMTA. But in addition to PN sequence, LS-DRMTCMA also utilizes the CM property of the transmitted signal that brings additional advantages and complexity. . The most prominent advan-

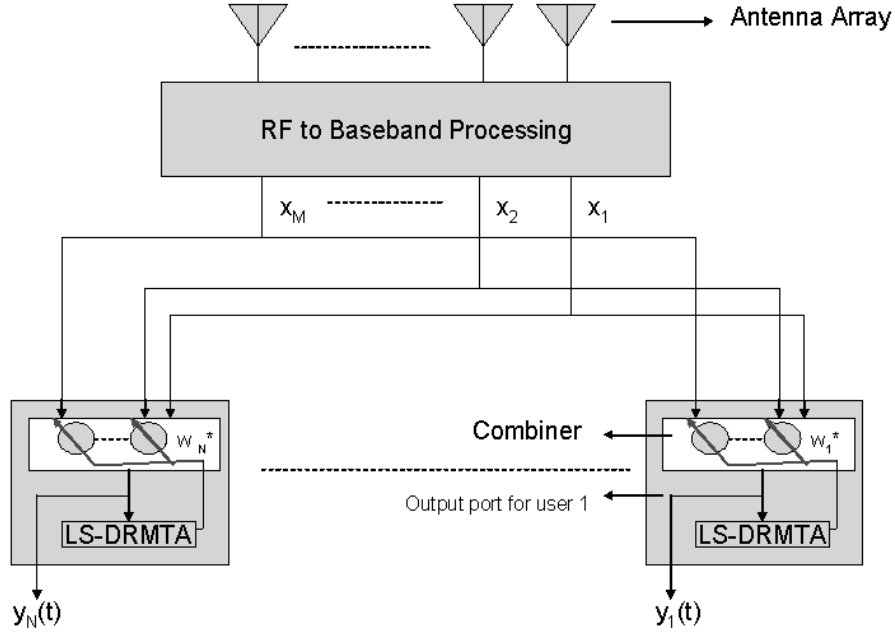


Figure 3.4: Structure of a BF using LS-DRTMA.

tage is that, since LS-DRMTCMA can generate deeper nulls in the antenna array pattern it has a better performance than LS-DRMTA . Structure of BF using LS-DRMTCMA is given in Figure 3.6

LS-DRMTCMA block diagram is shown in Figure 3.7. Similar to LS-DRMTA, LS-DRMTCMA tries to minimize the following cost function, but  $\mathbf{r}_i(k)$  now becomes the weighted sum of re-spread signal,  $\mathbf{r}_{i1}(k)$ , and complex-limited output,  $\mathbf{r}_{i2}(k)$

$$\begin{aligned}
 J(\mathbf{w}) &= \sum_{k=1}^K |y_i(k) - r_i(k)|^2 \\
 &= \sum_{k=1}^K |\mathbf{w}_i^H \mathbf{x}(k) - (a_1 \mathbf{r}_{i1}(k) + a_2 \mathbf{r}_{i2}(k))|^2
 \end{aligned} \tag{3.4}$$

$a_1$  and  $a_2$  determines the contribution of each part and satisfies the following equation

$$a_1 + a_2 = 1 \tag{3.5}$$

and the term  $\mathbf{r}_{i2}$  is obtained by dividing the output to its absolute value

$$\mathbf{r}_{i2}(k) = \frac{y_i(k)}{|y_i(k)|}. \tag{3.6}$$

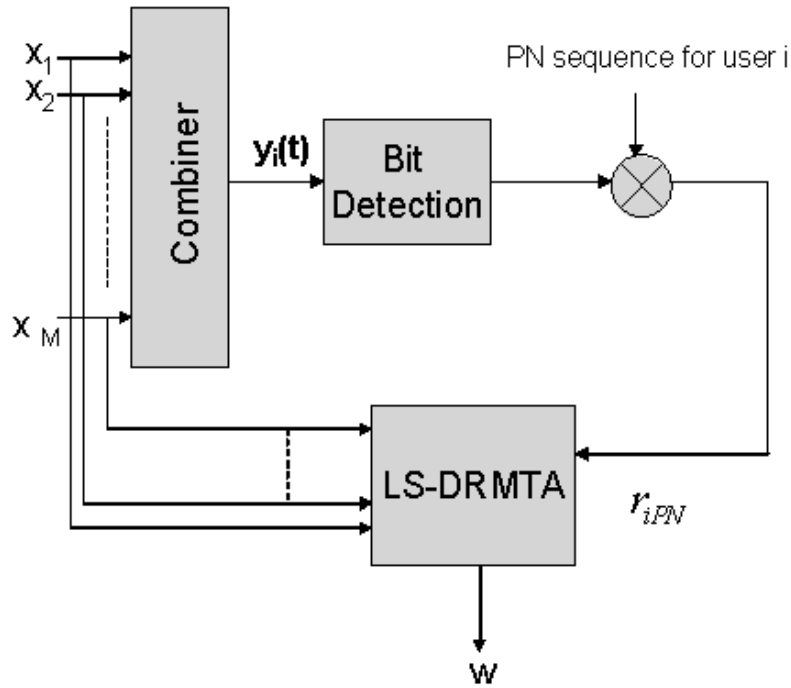


Figure 3.5: LS-DRMTA block diagram.

Similarly, the solution to Equation 3.4 is found by least squares solution and the weights are iterated by the following equation,

$$\mathbf{w}(l+1) = [\mathbf{X} \mathbf{X}^H]^{-1} \mathbf{X} \mathbf{r}_i^*. \quad (3.7)$$

where  $\mathbf{X}$  is a matrix containing  $K$  snapshot of array input data vector in each column. After each bit detection, the weights are adjusted by the Equation 3.7 until the algorithm converges.

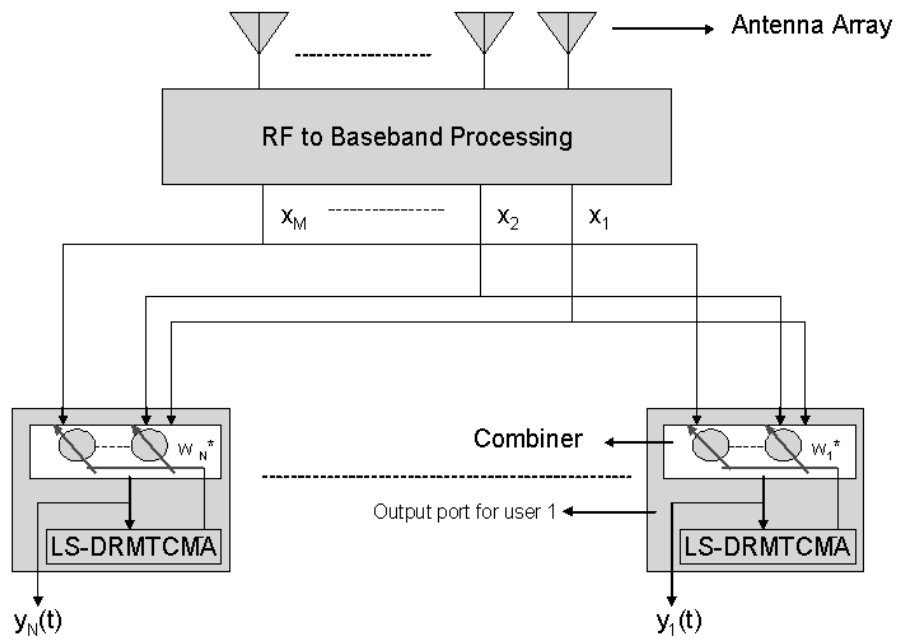


Figure 3.6: Structure of a BF using LS-DRMTCMA.

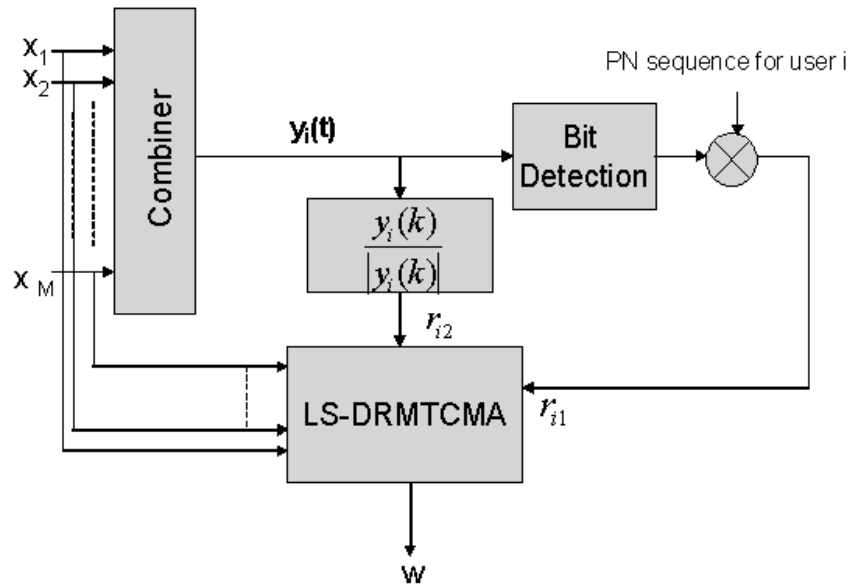


Figure 3.7: LS-DRMTCMA block diagram.

# Chapter 4

## Results and Discussions

### 4.1 Introduction

As it was stated in the preceding chapters, a smart antenna test-bed has been set up in a laboratory environment to evaluate the effects of frequency and time offsets on LS-DRMTA and LS-DRMTCMA experimentally. In this chapter, the properties of the set-up and the experimental results will be presented. Analysing the results, the performance of LS-DRMTA and LS-DRMTCMA in timing and frequency offset cases will be discussed.

### 4.2 The Smart Antenna Test-Bed

The smart antenna test-bed consists of two transmitters, representing two mobile users, and the receiver system as shown in Figure 4.1. In the receiver system, there is a two-element antenna array and each element is connected to a digital receiver that makes the conversion from RF to baseband. The transmitters generate RF signal at 2.125 GHz using signal generators as shown in Figure 4.2. The set up is a simple implementation of a W-CDMA system.

The position of the transmitter that radiates the SOI, Tx-1, is fixed, however the position of interferer, Tx-2, was changed as shown in the Figure 4.1. The angles between Tx-1 and Tx-2 are 70, 45, 30, 15 degrees. For each angle the samples were taken for SIR, the ratio of signal power radiated by Tx-2 to interferer power radiated by Tx-1, values of 0, -2, -4, -6, -8, -10 dB.

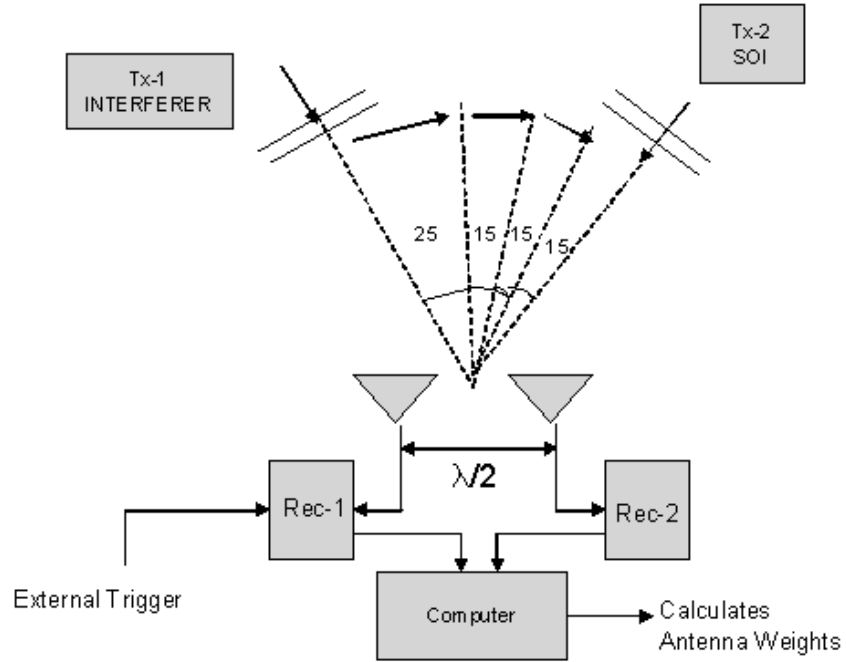


Figure 4.1: The test-bed includes two transmitters and a receiver system.

The digital receivers, in Figure 4.3 are wideband ( $BW = 20$  MHz) and the operating frequency is set to 2.125 GHz. After converting RF signal to baseband, the baseband signal is sampled at 40Msample/s with 10 bit precision. Then the samples are sent to computer for post processing in Matlab.

All the antennas used in the test-bed are microstrip inset-patch antennas. The antennas are designed to operate at 2.125 GHz. In the antenna array used in the receiver side, the antennas are separated by half-wavelength, 7 cm. The antennas are rectangular patch with the dimensions  $4mm \times 4.7mm$ .

The processing gain, number of chips per bit, used in the system,  $N_c$ , is 8. OVSF codes are chosen as , at

- DPDCH : 1 1 1 1 1 1 1 1
- DPCCH : 1 -1 1 -1 1 -1 1 -1.

A known data sequence is transmitted repeatedly to facilitate calculation of BER, for DPDCH channel 1 1 -1 1 -1 -1 1 1 -1 1 -1 -1 1 1 -1 -1 1 -1 1 -1 -1 1 1 -1 1 -1 -1 1 1 -1 1 -1 1 1 -1 1 -1 1 -1 and in DPCCH channel, always 1 is transmitted. Scrambling code is not used since generation and detection of scrambling codes increases the complexity of the set-up. The modulation scheme used in the set-up is Quadrature Phase Shift Keying (QPSK). The carrier frequency of the signal is 2.125 GHz and the chip rate is 2.5 Mcps. The sampling rate is four times the chip rate. The block size,  $K$ , used in the LS-DRMTA and LS-DRMTCMA is,  $8 \times 4 = 32$ . In LS - DRMTCMA, parameter  $\alpha_{CM}$  was set to  $1/3$  and  $\alpha_{PN}$  was  $2/3$ . since these are the optimum weights as shown in [3].

The baseband pulse shape used in the system is a Gaussian pulse with  $BT = 0.5$ , where  $B$  is the bandwidth of the Gaussian pulse and  $T$  is the symbol period.



Figure 4.2: The transmitter.

LS-DRMTA and LS-DRMTCMA are first designed for DS-CDMA, but it can be adapted for W-CDMA easily. The only difference is that in W- CDMA, spreading

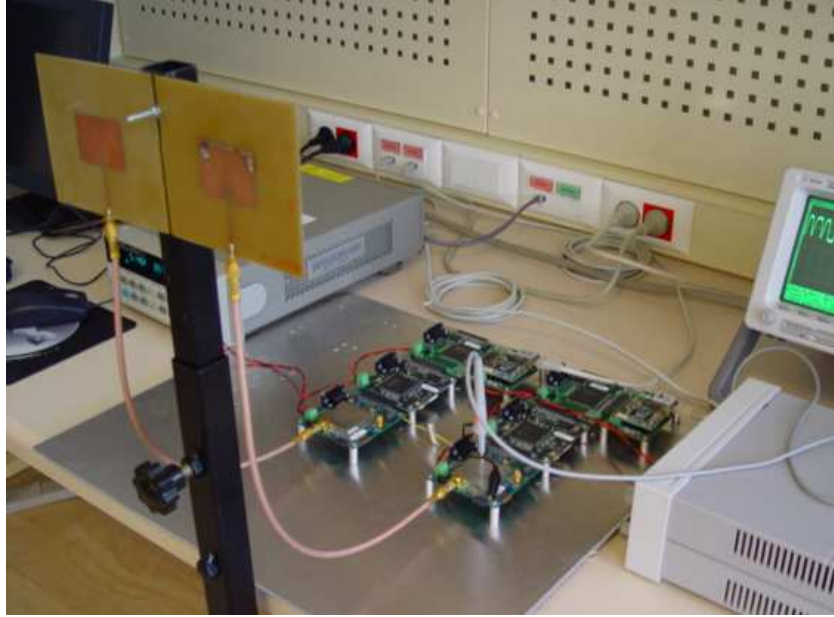


Figure 4.3: The receiver system.

de-spreading operations are done at both I and Q channels.

The digitized data is sent to the computer. After downloading the data, it is transferred to Matlab environment. In Matlab, first the phase rotation on the baseband samples, caused by the slight frequency offset, is removed. Then the two receivers are synchronized using the correlation between the known data sequence and the received data. Then the LS-DRMTA and LS-DRMTCMA are applied to the received data.

### 4.3 Results

After the implementation of LS-DRMTA and LS-DRMTCMA, according to the computed weights,  $w$ , baseband samples from the two receivers are combined, as shown in the Figure 4.4. As seen in Figure 4.4.a and 4.4.b, the baseband outputs of the antennas are quite corrupted due to interference, however combined signal using LS-DRMTA, 4.4.c, has a better signal quality since the interference is suppressed

by the algorithm.

Using the weights it is possible to plot the corresponding array pattern, as shown 4.5, or using the combined signal, bit error rate (BER) curves can be plotted. In this section, according to the test-bed output BER curves in three cases, frequency offset, timing offset and without frequency and timing offset case are plotted and the performance of conventional receiver, LS-DRMTA and LS-DRMTCMA is compared. In conventional receiver, only one antenna output is used and after despreading the bits are detected directly.

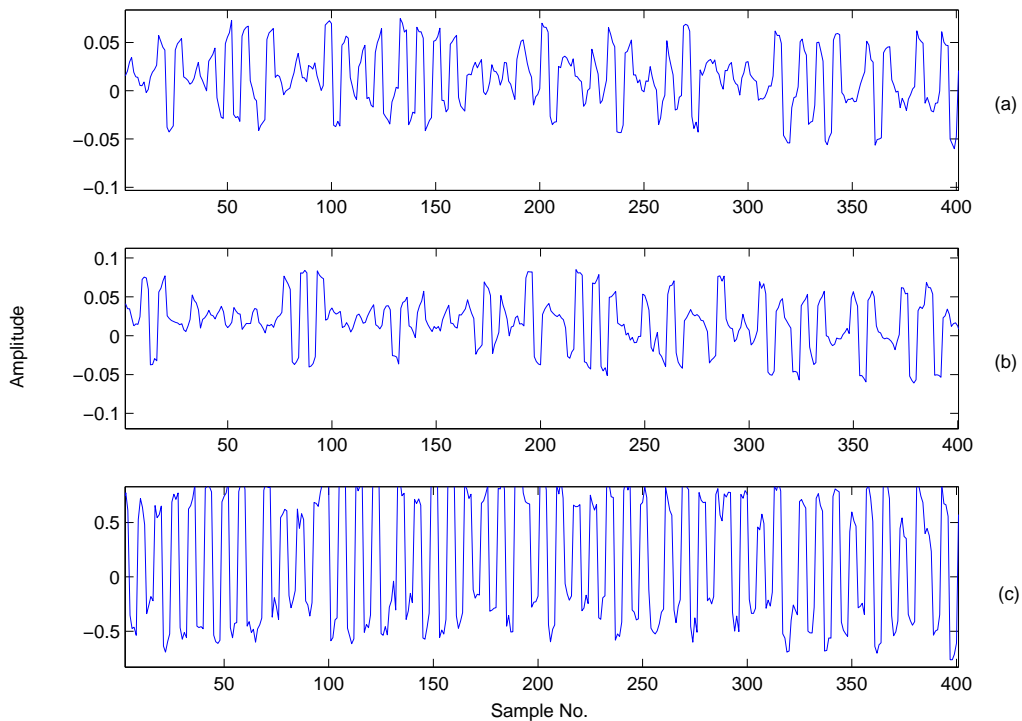


Figure 4.4: (a) Baseband I channel output of the first antenna. (b) Baseband I channel output of the second antenna. (c) Combined signal. In this case  $SIR = -8\text{dB}$ , the angle between SOI and interferer is  $45^\circ$

### 4.3.1 BER Performance without Frequency and Timing Offset

In this section the BER performance of conventional receiver, LS-DRMTA and LS-DRMTCMA will be compared in the condition when there is no timing and no

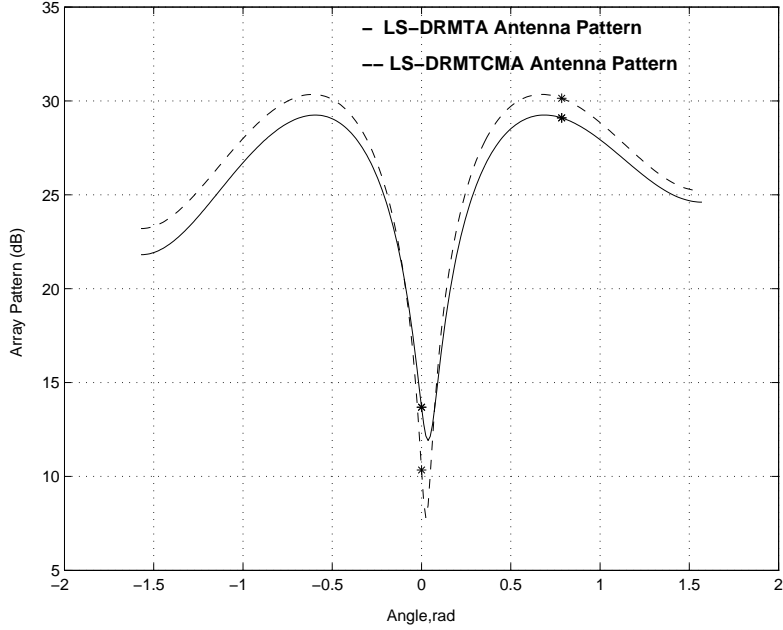


Figure 4.5: Antenna array pattern corresponding to the weights computed by LS-DRMTA and LS-DRMTCMA. In this figure the angle separation is  $45^{\circ}$ , and SIR = -4dB.

frequency offset exists. BER vs SIR curves will be plotted for SIR values of -4, -6,-8 and -10.

BER performance of the LS-DRMTA and LS-DRMTCMA, respectively, is shown in Figure 4.6 and Figure 4.7 and in Table 4.1. From the Figures 4.6 and 4.7 it can be seen that the BER increases as the SIR decreases, and LS-DRMTA and LS-DRMTCMA have much better performance than a conventional receiver. The reason for this is that, in a conventional receiver only one antenna output is used to detect the symbols, however in LS-DRMTA and LS-DRMTCMA two antenna outputs are combined before detection, in order to block the interfering signal. As seen in the Figure 4.5, using the weights computed by LS-DRMTA and LS-DRMTCMA, the interference can be suppressed by 15 dB and 20 dB, respectively.

As shown in the Figures 4.6 and 4.7, as the angle separation between SOI and interfering signal decreased, BER increases. This is due to peak to null BW of the

antennas, from the equation ??, the peak to null beamwidth of the main beam of the 2-element ULA is approximately

$$\theta_H = \sin^{-1}\left(\frac{\lambda}{Md}\right) = \sin^{-1}\left(\frac{\lambda}{2\lambda/2}\right) = 90^\circ \quad (4.1)$$

Since the angles  $15^\circ, 30^\circ, 45^\circ$  are smaller than  $90^\circ$ , the interfering signal falls into the main beam. Then, as the angle separation between SOI and interfering signal decreased, the array response in the direction of the interfering signal increases. As a result SIR decreases and BER increases.

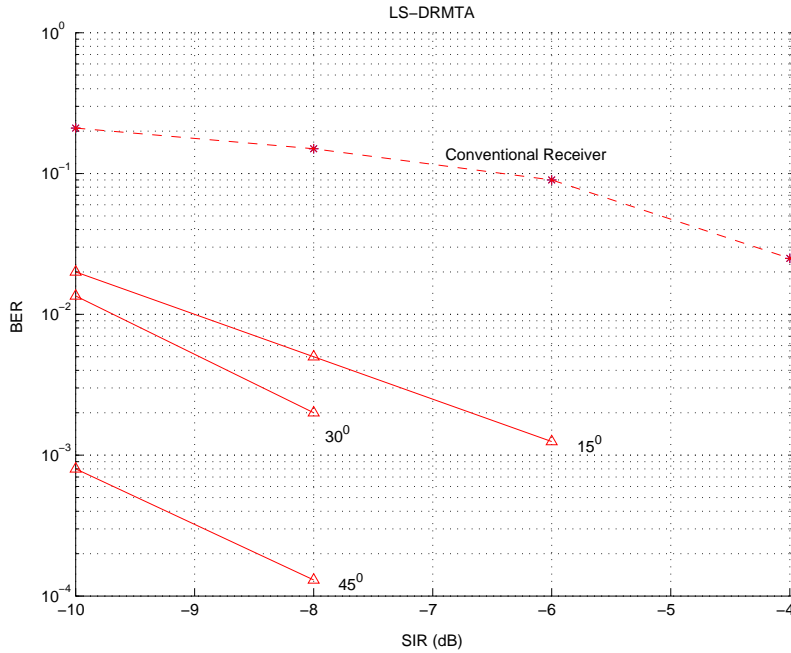


Figure 4.6: BER vs. SIR of conventional receiver and LS-DRMTA for different angle separations.

For all angle separations,  $15^\circ, 30^\circ$  and  $45^\circ$ , LS-DRMTCMA has a better BER performance than LS-DRMTA. As it was stated in the preceding chapter, LS-DRMTA utilizes PN sequence of the user's only, however LS-DRMTCMA utilizes both the PN sequence and constant modulus property of the transmitted signal. Therefore, LS-DRMTCMA can generate deeper nulls resulting better SIR value. For the same

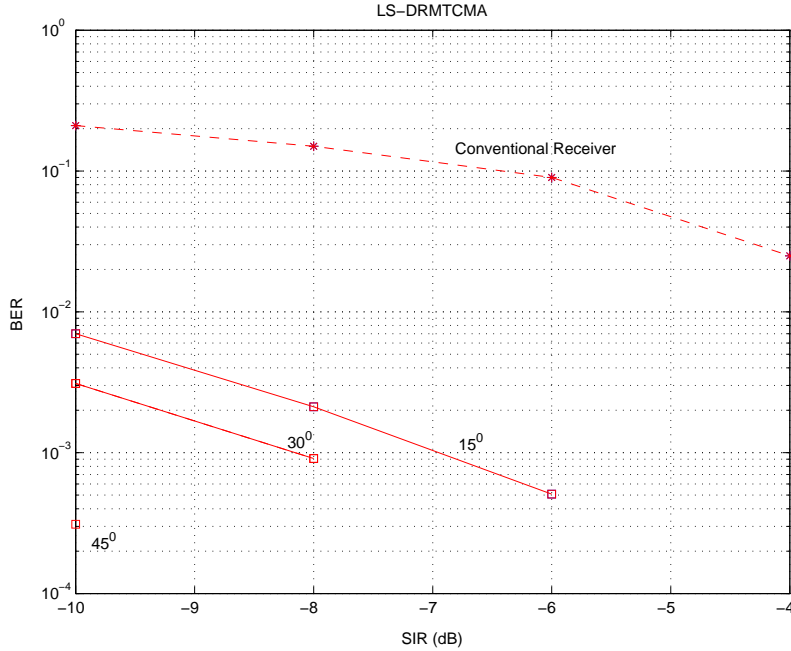


Figure 4.7: BER performance of conventional receiver and LS-DRMTCMA for different angle separations

SIR values, LS-DRMTCMA has lower BER.

As seen from the Table 4.3.1, LS-DRMTCMA performs averagely three times better than LS-DRMTA.

### 4.3.2 BER Performance with Timing Offset

One of the factors that degrades the smart antenna performance is the timing offset. In a CDMA system due to imperfect synchronization caused by interference and low SNR, a timing offset  $T_0$  exists between local generated and the received PN sequence. In this section, performance of LS-DRMTA and LS-DRMTCMA algorithms in timing offset case will be investigated. Since we have four samples per chip, by shifting the samples, we can investigate , %25, %50, %75 ,%100 timing offset cases.

In Figure 4.8 and 4.9 ,accordingly, the BER performance of the LS-DRMTA and LS-DRMTCMA for %25 timing offset case is shown for different separation

Table 4.1: BER values in the case without timing and frequency offset.

SIR=-10 dB	Angle Separation	LS-DRMTA	LS-DRMTCMA
	15 <sup>0</sup>	2.10 <sup>-2</sup>	7.10 <sup>-3</sup>
	30 <sup>0</sup>	1, 34.10 <sup>-2</sup>	3, 2.10 <sup>-3</sup>
	45 <sup>0</sup>	8, 09.10 <sup>-4</sup>	3, 2.10 <sup>-4</sup>
SIR = -8 dB	15 <sup>0</sup>	5, 2.10 <sup>-3</sup>	2, 2.10 <sup>-3</sup>
	30 <sup>0</sup>	2.10 <sup>-3</sup>	9, 1.10 <sup>-4</sup>
	45 <sup>0</sup>	1, 34.10 <sup>-4</sup>	-

angles. Comparing the Figures 4.8, 4.9 and Figures 4.6, 4.7 BER performance of both algorithms degrades with respect to the case without timing offset. In LS-DRMTA, for the same BER, in 25% timing offset case, SIR values must be 2-3 dB more than as it is for without timing offset case, however for LS-DRMTCMA, this can be 1-2 dB.

Comparing Figure 4.8 and 4.9, it can be deduced that LS-DRMTCMA outperforms the LS-DRMTA in 25% timing case, BER's for the same SIR are presented on Table 4.2. However, as the timing offset is increased, the improvement of LS-DRMTCMA over LS-DRMTA decreases, and their BER curves resembles to each other as shown in Figure 4.10. Because, as the timing offset is increased, BER is dominated by timing offset.

In the Figure 4.10 for LS-DRMTA, BER increases drastically, from 1, 2.10<sup>-3</sup> to 0.16, when timing offset is %50. Since, we have chosen OVVSF as alternating 1's and -1's, for %50 timing offset local generated and the received PN sequence becomes orthogonal. Increasing timing offset as much as %75, %100 causes local generated and the received PN sequence to be reverse of the each other. Then, detected data sequence becomes completely the reverse of the received data sequence. Therefore, for %75, %100 timing offsets, the results get worse and BER's close to 1 as shown in Figure 4.10.

Figure 4.11 shows the variation of array pattern with the changing timing offset

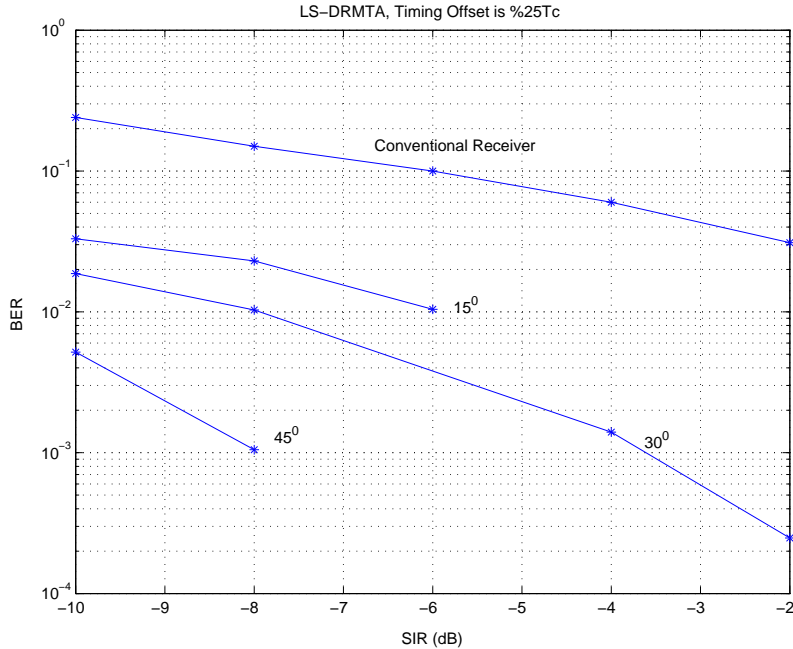


Figure 4.8: BER performance of LS-DRMTA and conventional receiver in 25% timing offset case.

values in LS-DRMTCMA. Comparing Figures 4.11.a and b, for 25% timing offset, suppression rate is 5 dB less than as it is for without the timing offset case. Although the timing offset is increased as much as 50%, 75% and 100%, interference suppression rate approximately stays the same around 15 dB. As a result, in spite of the serious timing offset, a reasonable SIR can be achieved for a better PN synchronization.

### 4.3.3 BER Performance with Frequency Offset

In a CDMA system, there may exist a frequency offset  $f_0$  between local oscillator and the carrier of the impinging signal. This will cause a phase rotation in baseband samples with the frequency related to  $f_0$ . If the frequency offset is not compensated, the BER performance of the receiver will be degraded seriously. In this section the BER performance of the conventional receiver, LS-DRMTA and LS-DRMTCMA will be investigated under the frequency offset conditions where

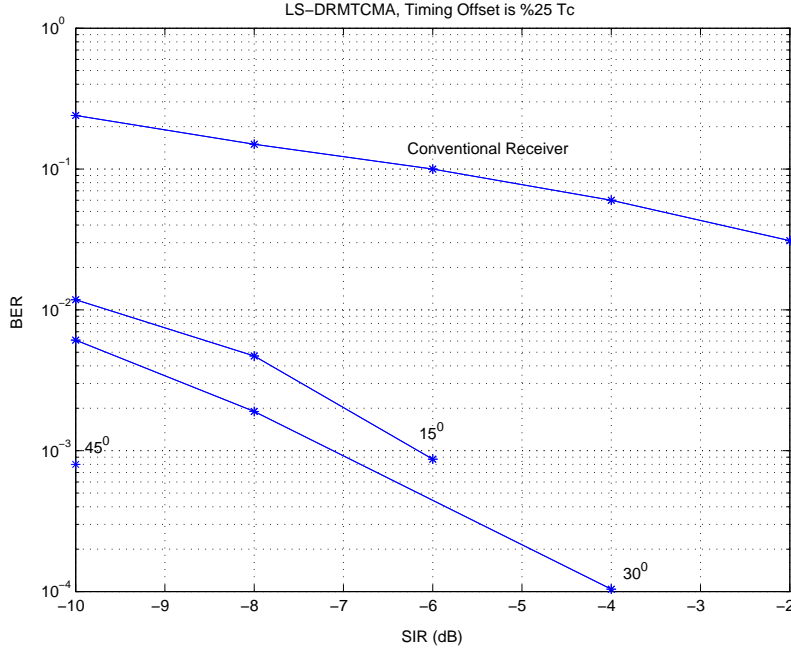


Figure 4.9: BER performance of LS-DRMTCMA and conventional receiver in %25 timing offset case.

$F_0 = 100Hz$  and  $F_0 = 500Hz$ . In order to have a frequency offset effect on the baseband samples, baseband samples are multiplied with the corresponding discrete frequency  $\omega_d$ ,  $\exp(j\omega_d n)$ , where  $n$  is an integer.

The frequency offset will cause the signal constellation to rotate along the unit circle with a speed proportional to the value of the frequency offset. If the frequency is not compensated, this leads to very high BER in PSK modulation schemes. In fact, the adaptive algorithm tries to restore the rotated signal constellation to the its closest one. Therefore, for the W-CDMA signal having QPSK constellation, Figure 4.12, if the adaptive algorithm can update the weight vector before the phase rotation exceeds  $\pi/4$ , i.e, before the constellation passing through the imaginary axis, then the constellation will be restored to the right one. So, for the W-CDMA the maximum allowable phase shift, denoted by  $\phi_a$ , between two consecutive adaptation may be given as

$$\phi_a < \pi/4. \quad (4.2)$$

Table 4.2: BER values in %25 timing offset case

SIR=-10 dB	Angle Separation	LS-DRMTA	LS-DRMTCMA
	15 <sup>0</sup>	0.33	1, 18.10 <sup>-2</sup>
	30 <sup>0</sup>	1, 87.10 <sup>-2</sup>	6, 1.10 <sup>-3</sup>
	45 <sup>0</sup>	5, 18.10 <sup>-3</sup>	8.10 <sup>-4</sup>
SIR = -8 dB	15 <sup>0</sup>	0.23	4, 7.10 <sup>-3</sup>
	30 <sup>0</sup>	1, 03.10 <sup>-2</sup>	1, 9.10 <sup>-3</sup>
	45 <sup>0</sup>	1, 5.10 <sup>-3</sup>	-

The choice of  $\phi_a$  determines the weight update frequency, and affects the performance of LS-DRMTA and LS-DRMTCMA.

In the Figure 4.13 and 4.14, the BER performance of LS-DRMTA and LS-DRMTCMA is shown for different separation angles. BER's in the Figure 4.13 and 4.14 is tabulated in Table 4.3. In these figures, the frequency offset is 100 Hz and  $\phi_a$  is set at  $0.1\pi$ . Comparing the Figures 4.13, 4.14 and Figures 4.6, 4.7 the BER performance of the conventional receiver degrades drastically. Also the performance of the LS-DRMTA and LS-DRMTCMA degrades, however they still give reasonable BER values since the weight update is sufficiently fast to restore the rotated signal constellation. For the same BER, in frequency offset case the performance of the both algorithms degrades 6-7 dB with respect to the case without timing or frequency offset. LS-DRMTCMA outperforms the LS-DRMTA in frequency offset condition.

As shown in the Figure 4.15, the BER does not change significantly with the frequency offset. In the figure increasing frequency offset from 100 Hz to 200Hz BER increases a little for both of the algorithms. Increasing the frequency offset beyond 300 Hz doesn't change BER significantly only it fluctuates weakly. Since increasing the frequency offset, will also increase the weight update frequency, as a result the BER performance of the algorithms will not change significantly.

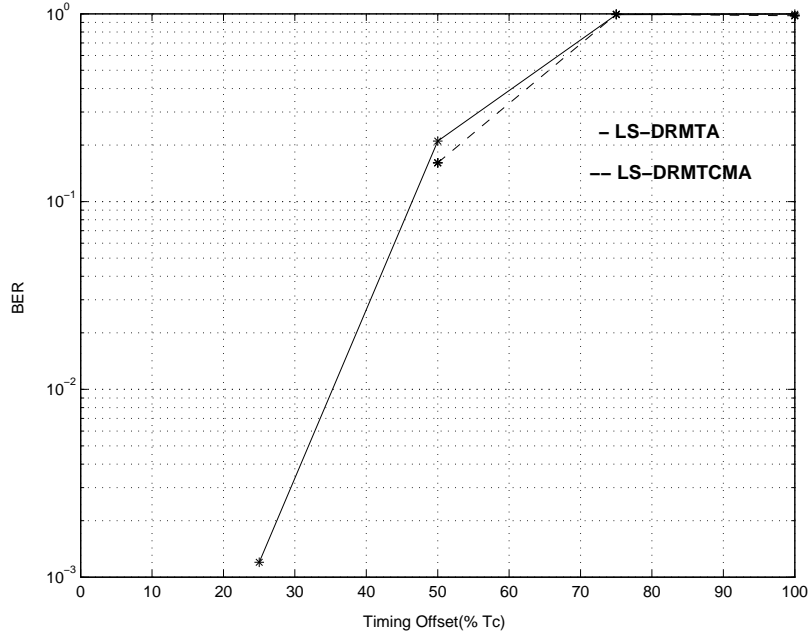


Figure 4.10: BER vs. timing offset . In this figure SIR = -8dB and angle separation is  $45^{\circ}$

In the Figure 4.16 and 4.17, the relation between the BER performance of the algorithms and the  $\phi_a$  can be seen. It can be seen that reducing the  $\phi_a$ , we can get lower BER values. For example, while angle separation is  $30^{\circ}$  and frequency offset is 100Hz, for LS-DRMTA BER decreases from  $9,8 \cdot 10^{-3}$  to  $5,2 \cdot 10^{-3}$  or for LS-DRMTCMA decreases from  $4,7 \cdot 10^{-3}$  to  $2 \cdot 10^{-3}$ , if  $\phi_a$  is reduced from  $0.1\pi$  to  $0.05\pi$ . However reducing  $\phi_a$  from  $0.1\pi$  to  $0.05\pi$  means increasing the weight update frequency two times, that results in a higher computational complexity. Therefore, there is a trade off between  $\phi_a$  and BER.

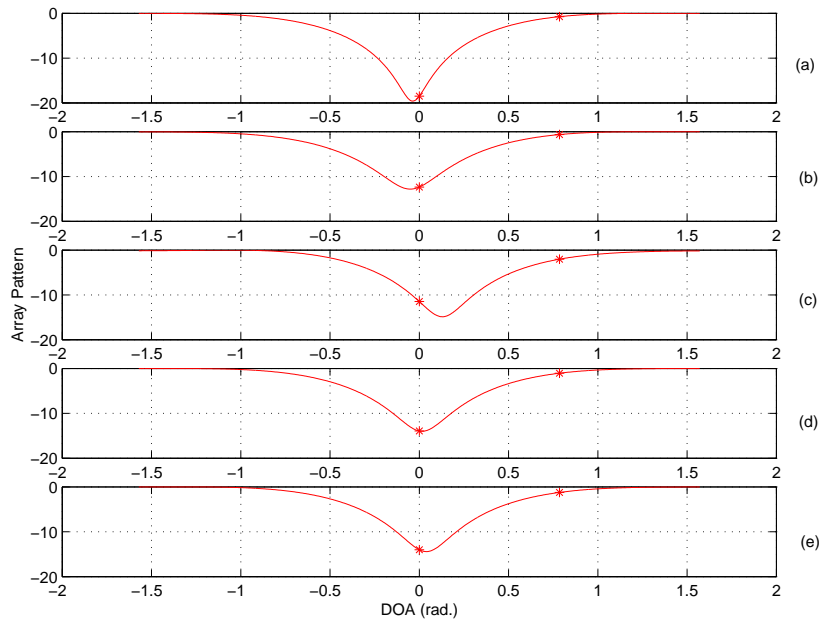


Figure 4.11: Array patterns for different timing offsets. (a)  $T_o = 0$ , (b)  $T_o = \%25T_c$ , (c)  $T_o = \%50T_c$ , (d)  $T_o = \%75T_c$ , (e)  $T_o = \%100T_c$ . In this figure  $SIR = -10$  dB and angle separation is  $45^\circ$

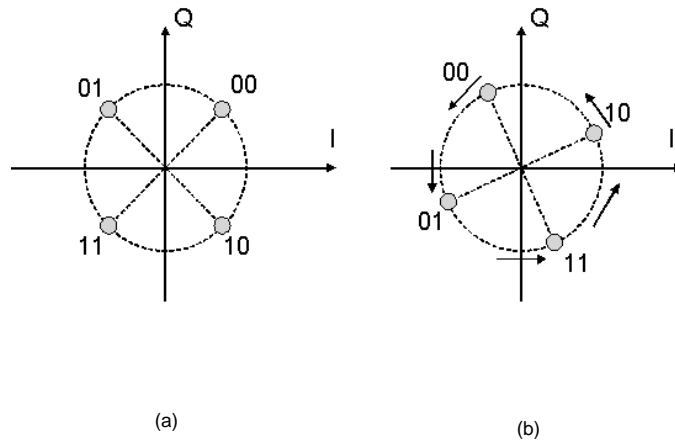


Figure 4.12: (a) QPSK Constellation. (b) Rotated QPSK constellation due to frequency offset.

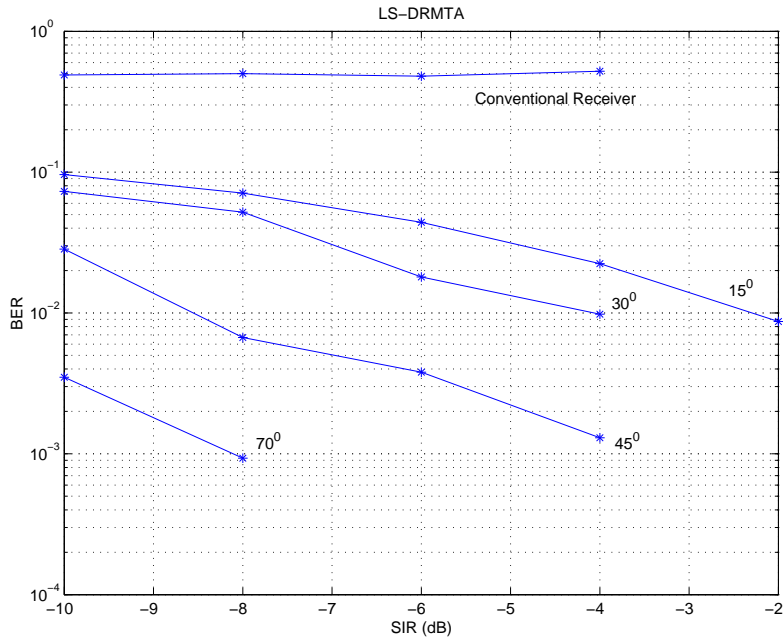


Figure 4.13: BER performance of conventional receiver and LS-DRMTA. In this figure the frequency offset is 100 Hz and  $\phi_a$  is set at  $0.1\pi$

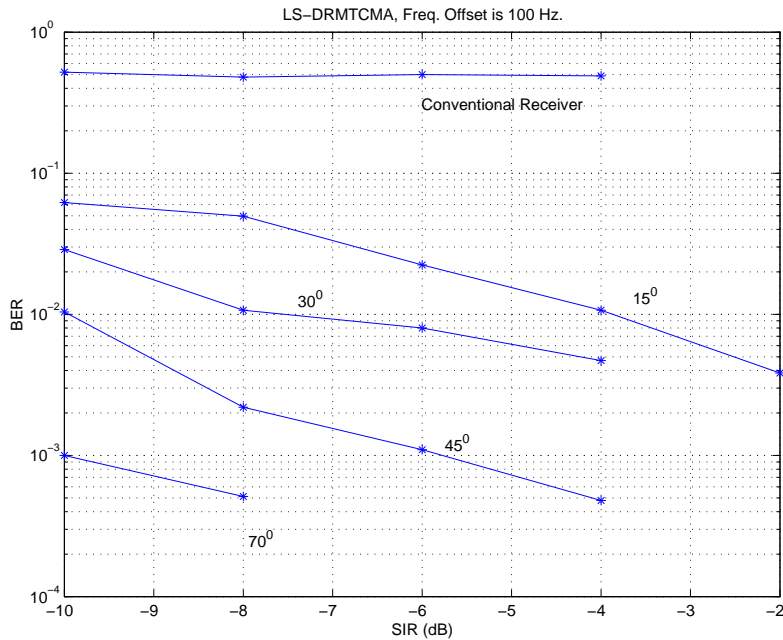


Figure 4.14: BER performance of conventional receiver and LS-DRMTCMA. In this figure the frequency offset is 100 Hz and  $\phi_a$  is set at  $0.1\pi$

Table 4.3: BER values in frequency offset case. In this table frequency offset is 100 Hz.

SIR = -10 dB	Angle Separation	LS-DRMTA	LS-DRMTCMA
	$15^0$	$9, 6 \cdot 10^{-2}$	$6, 2 \cdot 10^{-2}$
	$30^0$	$7, 3 \cdot 10^{-2}$	$2, 8 \cdot 10^{-2}$
	$45^0$	$2, 8 \cdot 10^{-2}$	$1, 04 \cdot 10^{-2}$
	$70^0$	$3, 5 \cdot 10^{-3}$	$10^{-3}$
SIR = -8 dB	$15^0$	$7, 1 \cdot 10^{-2}$	$4, 96 \cdot 10^{-2}$
	$30^0$	$5, 2 \cdot 10^{-2}$	$1, 07 \cdot 10^{-2}$
	$45^0$	$6, 7 \cdot 10^{-3}$	$2, 2 \cdot 10^{-3}$
	$70^0$	$9, 32 \cdot 10^{-4}$	$5, 12 \cdot 10^{-3}$
SIR = -6 dB	$15^0$	$4, 4 \cdot 10^{-2}$	$2, 24 \cdot 10^{-2}$
	$30^0$	$1, 8 \cdot 10^{-2}$	$8 \cdot 10^{-3}$
	$45^0$	$3, 8 \cdot 10^{-3}$	$1, 1 \cdot 10^{-3}$
	$70^0$	-	-

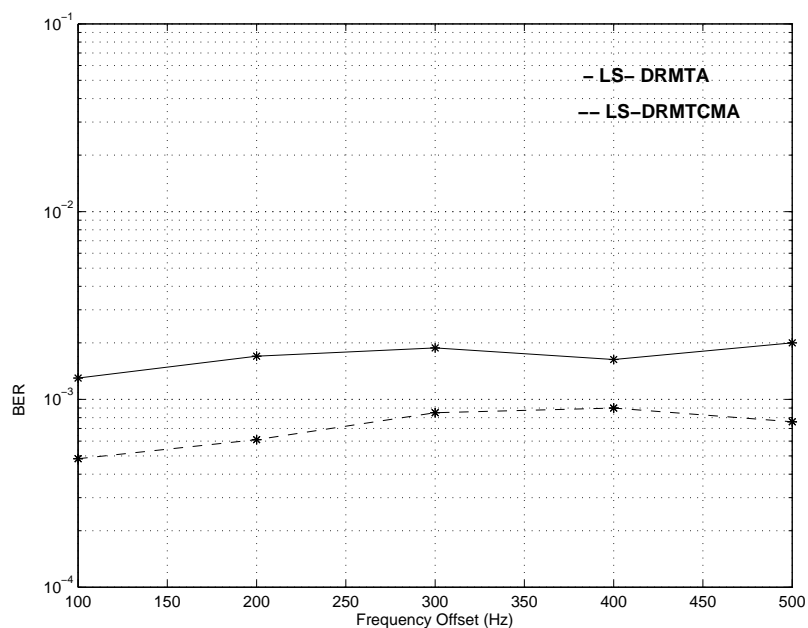


Figure 4.15: BER vs frequency offset. In this figure, angle separation between the users is  $45^0$ , SIR = -4 dB and  $\phi_a$  is set at  $0.1\pi$ .

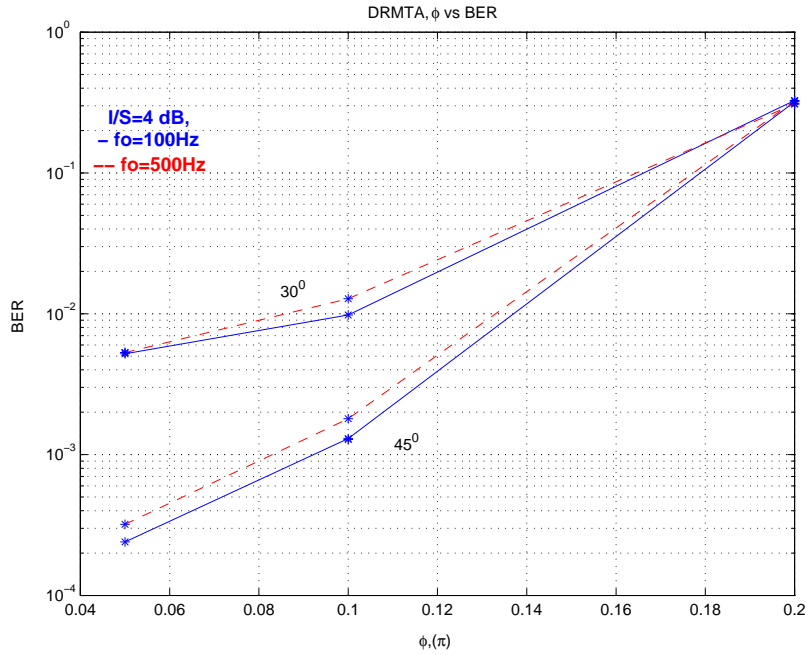


Figure 4.16: BER vs  $\phi_a$  for the LS-DRMTA algorithm. In this figure, SIR = -4 dB, the angle separation is  $30^\circ$  and  $45^\circ$ .

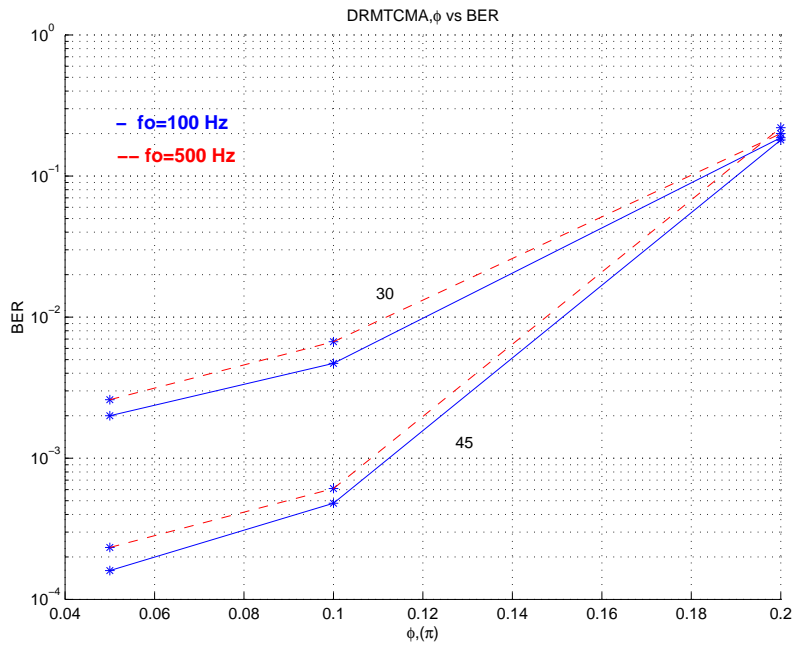


Figure 4.17: BER vs  $\phi_a$  for the LS-DRMTCMA algorithm. In this figure, SIR = -4 dB, the angle separation is  $30^\circ$  and  $45^\circ$ .

## Chapter 5

### Conclusion

In this thesis, BER performance of LS-DRMTA, LS-DRMTCMA and conventional receiver are compared using the outputs of a set-up in a laboratory environment. The set up is a simple implementation of a W-CDMA system that consists of two transmitters, representing two mobile users, and a receiver system including a half-wavelength spaced two-element antenna array connected to digital receivers. The output of the receivers, sampled and digitized baseband data, is sent to a computer to implement the smart antenna algorithms. BER performance of LS-DRMTA, LS-DRMTCMA and conventional receiver compared in three cases, without frequency and timing offset case, frequency offset case and timing offset case. In each case, the samples are taken for the angle separation of  $15^\circ$ ,  $30^\circ$ ,  $45^\circ$  and  $70^\circ$  between interferer and desired user. Furthermore, for each angle the samples are taken for the SIR values of -10, -8, -6, -4, -2 and 0 dB.

It was shown from the BER curves, in all test conditions LS-DRMTA and LS-DRMTCMA outperforms conventional receiver. LS-DRMTA and LS-DRMTCMA can suppress the interference 15-20 dB, but LS-DRMTCMA can generate deeper nulls in the antenna array pattern than LS-DRMTA as a result LS-DRMTCMA outperforms LS-DRMTA in all test conditions. Frequency offset and timing offset degrades the performance of the LS-DRMTA and LS-DRMTCMA, however they still have reasonable BER and performs better than a conventional receiver. Increasing the frequency offset effects BER slightly if the weight update frequency

is increased proportional to the frequency offset, on the other hand increasing the timing offset beyond  $0.25T_c$  causes the BER to increase drastically although interference suppression rate is good enough, this is because of the BER is dominated by the timing offset. In all test conditions, decreasing the angle separation from  $70^\circ$  to  $15^\circ$  increases the BER for both of the algorithms. Moreover, decreasing the SIR value causes the BER to increase for both of the algorithms in all test conditions, however they can still work at low SIR conditions as much as -10 dB .

In conclusion, smart antennas can be a good solution for capacity increase, since it lessens the effects of interference between the users, that is the major handicap limiting the capacity of the CDMA systems.

A few possibilities for future works based on the results of this thesis can be enumerated as follows.

- In this thesis, BER performance of LS-DRMTA, LS-DRMTCMA and conventional receiver are compared using the outputs of a set-up in a laboratory environment. A similar system can be simulated and the results can be compared.
- We only used a set-up involving 2-user and 2-element antenna array. A larger antenna array having more than 2 elements can be used. Similarly, a set-up having more than 2 users can be used to examine the overloaded case.
- In this research, a full implementation of W-CDMA is not used. Scrambling code is not used and short OVSF code (only 8 chips per bit) is used. The performance of the algorithms can be investigated in a set-up using fully implemented W-CDMA signal.
- The antennas in this research are linearly configured and rectangular patch antennas. The performance of different antenna types and array configuration schemes can be examined.
- In this thesis, only the algorithms are examined for W-CDMA uplink. The

performance of the algorithms can be evaluated for downlink. The relation between uplink and downlink BF weights can be examined, because generally uplink and downlink carrier frequencies are different.

# Bibliography

- [1] T. Ojanpara and R. Prasad, Wideband CDMA for 3G mobile communications, Artech House, 1998.
- [2] W. L. Stutzman and G. A. Thiele, Antenna Theory and Design, John Wiley & Sons, 1998.
- [3] B. G. Agee, "Blind separation and capture of communication signals using a multitarget constant modulus beamformer," Proc. IEEE Military Communication Conf., 1989.
- [4] Z.Rong, "Simulation of MultiTarget Adaptive Algorithms for Wireless CDMA systems" Proc. IEEE Vehicular Technology Conf., April 1996.
- [5] C.Balanis, Antenna Theory, John Wiley & Sons, 1997.
- [6] B. D. Van Veen and K. M. Buckley, " Beamforming: A versatile approach to spatial filtering," IEEE ASSP Magazine, pp. 4-24, April 1988.
- [7] T. Macnamara, "Simplified design procedure for Butler Matrices incorporating 90 and 180 hybrids," IEEE Proc. Microwave and antenna and Prop., pp. 50-54, 1987
- [8] R. A. Monzingo and F. Amoroso, Introduction to adaptive arrays, John Wiley & Sons, 1980.
- [9] A. O. Boukalov and S. G. Haggman, " System Aspects of Smart Antenna Technology in Cellular Wireless Communications, " IEEE Trans. on Microwave Theory and Tech., vol. 48, no. 6, pp. 919-922, June 2000.

- [10] J. Capon, "High resolution frequency-wave analysis," *Proc. IEEE*, vol. 57, pp. 1408-1418, 1969.
- [11] L. C. Godara "Application of antenna arrays to mobile communications : Part 2," *Proc. IEEE*, vol. 85, no. 6, pp. 1193-1245, August 1997.
- [12] R. O. Schmidt, "Multiple emitter location and signal parameter estimation," *IEEE Trans. Antennas Propagat.*, vol. AP-34, pp. 276-280, 1986.
- [13] R. Roy and T. Kailath, "ESPRIT-Estimation of signal parameters via rotational invariance techniques," *IEEE Trans. Acoust., Speech, Signal Processing*, vol. ASSP-37, pp. 984-995, 1989.
- [14] W. Du and R. L. Kirlin, "Improved spatial smoothing techniques for DOA estimation of coherent signals," *IEEE Trans. Signal Processing*, vol.39, pp. 1208-1210, 1991.
- [15] T. S. Rappaport and J. C. Liberti, *Smart antennas for wireless communications*, Prentice Hall, 1999.
- [16] I. Ziskind and M. Wax, "Maximum likelihood localization of multiple sources by alternating projection," *IEEE Trans. Acoust., Speech, Signal Processing*, vol. ASSP-36, pp. 1553-1560, 1988.
- [17] D. T. M. Slock, "On the convergence behavior of the LMS and the normalized LMS algorithms," *IEEE Trans. Signal Processing*, vol. 41, pp. 2811-2825, 1993.
- [18] S. Qiao, "Fast adaptive RLS algorithms: A generalized inverse approach and analysis," *IEEE Trans. Signal Processing*, 39, pp. 1455-1459, 1991.
- [19] J. R. Treichler and B. G. Agee, "A new approach to multipath correction of constant modulus signals," *IEEE Trans. Acoust., Speech, Signal Processing*, vol. ASSP-31, pp. 459-472, 1983.
- [20] B. G. Agee, "The Least-Squares CMA: A new technique for rapid correction of constant modulus signals," *Proc. IEEE ICASSP*, 1986.

- [21] S. Talwar, M. Viberg and A. Paulraj, "Blind estimation of multiple co-channel digital signals arriving at an antenna array," proc. 27th. Asilomar Conf. on Signals, Systems and Computers, vol. 1, pp 349-353, November 1993.
- [22] S. S. Jeon, Y. Wang, Y. Qian, "A novel smart antenna system implementation for broad-band wireless communications," IEEE Trans. Antennas and Propag., vol. 50, no. 5, May 2002.
- [23] S. Denno, T. Ohira, "Modified constant modulus algorithm for digital signal processing adaptive antennas with microwave analog beamforming IEEE Trans. Antennas and Propag., vol. 50, no. 6, June 2002.
- [24] K. R. Daandekar, H. Ling, G. Xu, "Experimental study of mutual coupling compensation in smart antenna applications" IEEE Trans. Wireless Comm., vol. 1, no. 3, July 2002.
- [25] K. Kim, T. K. Sarkar, M. S. Palma, " Adaptive processing using a single snapshot for a nonuniformly spaced array in the presence of mutual coupling and near-field scatterers," IEEE Trans. Antennas and Propag., vol. 50, no. 5, May 2002.
- [26] J. G. Proakis, Digital Communications, Prentice Hall, 2000.